Journal of Polymers and the Environment
https://doi.org/10.1007/s10924-025-03563-y

ORIGINAL PAPER

Physical and Electrical Properties of Polylactic Acid-Based Adsorbents for the Malachite Green Dye Removal with Potential Sensoric Application

Khadiga Mohamed Abas[1] · Miroslav Mrlik[2] · Katarína Mosnáčková[3] · Jaroslav Mosnáček[3,4]

Accepted: 20 March 2025

Abstract

New adsorbent films for the biosorption of malachite green (MG) dye from water were prepared using polylactic acid (PLA) as a renewable, degradable and thermoplastic polymer matrix, instead of widely used crosslinked systems. Polyaniline (PANI) and carbon fibers (CFs) were added to PLA through vigorous sonication followed by a casting technique to create electrically conductive PLA-based adsorbent films with enhanced functionality and adsorption properties. The composite films were characterized using scanning electron microscopy, Fourier transform infrared spectroscopy, differential scanning calorimetry, dynamic mechanical thermal analysis, and BET-surface area measurements to identify their functionality as adsorbents for removing MG dye from water. The produced PLA/PANI/CFs composite films exhibited higher electrical conductivity and surface area compared to PLA and PLA/PANI films. The effects of adsorbent film composition, contact time, pH, and dye concentration on adsorption efficiency were assessed. The adsorption test confirmed effective removal of MG dye with maximum adsorption capacities of up to 60.1 mg/g. The isotherm data fitted the Langmuir model with an R^2 value of 0.99, implying a chemisorption process. The fabricated biosorbents disclosed the first-order kinetic model with high R^2 values and an exothermic reaction with the MG dye, as the process is stimulated by a decrease in temperature. Adsorbent regeneration and the significant effect of various MG concentrations on electric conductivity, which changed by two orders of magnitude, demonstrated the applicability of PLA/PANI/CFs composite films as potential MG dye sensors.

Keywords Polylactide · Polyaniline · Carbon Fibers · Polylactide-based Films · Biosorption

✉ Katarína Mosnáčková
katarina.mosnackova@savba.sk

✉ Jaroslav Mosnáček
jaroslav.mosnacek@savba.sk

Khadiga Mohamed Abas
mohamedkhadiga728@yahoo.com; km.hassan@nrc.sci.eg

Miroslav Mrlik
mrlik@utb.cz

[1] Physical Chemistry Department, Advanced Materials Technology and Mineral Resources Research Institute, National Research Centre, 33 El-Bohouth St, Giza 12622, Egypt

[2] Centre of Polymer Systems, University Institute, Tomas Bata University in Zlín, Trida T. Bati 5678, Zlín 76001, Czech Republic

[3] Polymer Institute of the Slovak Academy of Sciences, Dúbravská cesta 9, Bratislava 845 41, Slovakia

[4] Centre for Advanced Materials Application of the Slovak Academy of Sciences, Dúbravská cesta 9, 845 11, Bratislava, Slovakia

Published online: 02 April 2025

Introduction

Nowadays, the organic dyes are extensively used as coloring agents for fabric, leather, plastics, and paper. With the increasing consumption in the dyestuff and pigment industry, there is an extensive increase in water contamination by synthetic non-biodegradable dye residues, which represents serious environmental problems [1]. Malachite green (MG) dye is an organic compound based on triarylmethane characterized by high stability, non-biodegradability, and high resistance to light and oxidizing agents. MG is commonly used as a dye for materials such as silk, cotton, leather, wool and paper. Due to its high solubility in water, the contamination of wastewater with MG represents a serious environmental hazard. MG dye is mutagenic for humans and affects the immunological and reproductive systems. It is also highly toxic to mammalian cells and influences photosynthesis and plant growth, thereby affecting the biological activity of living organisms in water [2]. Typically, the principal techniques used for dye removal involve physical or chemical processes, including membrane separation, adsorption, ion exchange, oxidation, coagulation, and flocculation. Adsorption is considered one of the most effective approaches for wastewater treatment because it is fast and easy to exploit [3–5]. It permits variability in both design and operation, additionally it produces pollutant-free effluents suitable for reuse. The adsorption process has considerable advantages compared to conventional methods, particularly from technical, economic, and environmental perspectives. Among other techniques, adsorption has proven to be an effective route with high efficiency, capacity and large-scale applicability for eliminating dyes. It also offers potential for the regeneration, recovery and recycling of adsorbents [6].

The prevalence of monomers generated from fossil sources has played a major role in the establishment of many products used in daily life, business, agriculture, and other industries. Serious environmental problems are caused by the extensive use of these products and the accumulation of plastic waste in landfills. In addition to the plastic pollution problem, it is highlighted that the world's petroleum reserves are becoming limited due to increased demand from different industries. Plastics offer several advantages but can be reprocessed, dumped, or discarded in the environment, with or without alteration. In 2013, 32% of the 78 million tons of plastic waste ended up in the environment [7]. Biopolymers appear to be a suitable alternative for petrochemical polymers in several applications. Among all bioplastics used worldwide in 2010, polylactic acid (PLA) had the second-greatest volume of consumption [8]. It is a biodegradable polyester derived from renewable resources, and thanks to its thermoplastic behavior and good processability, it has already emerged widely in various packaging applications such as bottles, films, and cups [9]. By imparting certain qualities to PLA, such as conductivity [10], antimicrobial properties [11] and UV resistance [12], it has been the focus of numerous studies in recent years. However, in most cases, thermoplastics do not possess the properties required for the adsorption of certain types of water pollutants. These are mostly based on either chemically crosslinked systems with the absence of reusability [13, 14] or as a hybrid particle systems [15, 16]. Mixing thermoplastics with other polymers or fillers is necessary to ensure their suitability for water treatment. To enhance the physical and adsorption properties of PLA, polymers (PEG, PPG) [17], charged conductive polymers (polyaniline (PANI), polypyrrole (PPy)) [18, 19], fillers (graphene oxide [20], activated carbon [21], silicone dioxide [17], carbon fibers (CFs) [22], carbon nanotubes [23]), and other additives are commonly used.

PANI has garnered significant attention worldwide due to its simple preparation, good electrical conductivity, and environmental stability [24, 25]. Moreover, aniline has recently been derived from biomass [26] instead of a petrochemical precursor through sugar fermentation [27] and commercialized by Covestro company. The PANI chain interacts efficiently via amine and imine functional groups with organic dye molecules, facilitating their removal from wastewater. Recently, many published studies have reported the use of PANI and its composites as efficient adsorbents for water treatment and purification from organic impurities [1, 28–32]. However, the combination of PLA with PANI results in deterioration of mechanical properties [33, 34]. Therefore, it is crucial to figure out an appropriate method for boosting PLA strength when paired with PANI filler.

Recent years have seen a number of studies conducted on thermoplastic/thermoset composites reinforced with carbon fibers (CFs) as a reinforcing filler through ex-situ processing [35, 36], because of their exceptional mechanical qualities, unique surface chemistry, high biocompatibility, and biodegradability. One of the most common sources for CFs production is lignocellulosic biomass. Cotton-based CFs (CCFs), with its hollow structure, can improve the electrochemical properties of the host material when applied as active fillers. Additionally, its application in wastewater remediation due to their high surface area [37]. It was found that incorporating high surface area functionalized fillers into polymers can effectively remove cationic organic pollutants from waste water [38–41]. S. J. Peighambardoust et al. investigated the effective removal of Malachite green dye using prepared carboxymethyl cellulose (CMC)/montmorillonite (MMT) nanocomposite hydrogels [42].

The main objective of this work was to develop a feasible approach for effective organic dye removal using composite films based on renewable thermoplastic polymer such as

PLA, with ability to be reprocessed/recycled. It was combined with PANI and CFs to obtain material with high dye adsorption capacity, good viscoelastic properties and electrical conductivity. Malachite Green (MG), a cationic dye, was studied for its removal efficiency by the PLA/PANI/CFs composite films. The effect of CFs loading on the electrical conductivity of PLA/PANI/CFs composite films was systematically surveyed, and the thermal properties of composites were estimated. The effects of pH and concentration of MG dye on the adsorbent efficiency were investigated. Additionally, kinetics, equilibrium as well as thermodynamics for the adsorption of MG dye onto the composite films were studied. Finally, the effect of adsorption of MG dye on changes in conductivity of the PLA/PANI/CFs composite film was proven.

Materials and Methods

Materials

Commercial polylactic acid (PLA) pellets used for the preparation of film matrix were supplied from Panara, s.r.o. (Nitra, Slovakia) ($M_n \approx 89$ kDa). The precursor for carbon fibers (CFs) used in this study is non-sterile waste cotton (WC) (MISR MEHALLA A.R.E.; Egypt). Nitric acid (HNO_3), dimethylsulfoxide (DMSO), ammonium persulfate ($(NH_4)_2S_2O_8$; APS), tetrahydrofuran (THF), and aniline (ANI) monomer were gained from Sigma-Aldrich company (Weinheim, Germany). Aniline monomer was distilled under vacuum before utilization. Malachite green (MG) dye (CID: 11294; chemical formula: $C_{23}H_{25}ClN_2$; molecular weight: 364.91 g/mol; maximum wavelength: 617 nm) was purchased from Sigma-Aldrich company. All chemicals were of analytical grade and used as received without further purification unless otherwise stated. The synthesis of PANI and the preparation of carbon fibers (CFs) from waste cotton are described in SI.

Elaboration of PLA-Based Composites

To fabricate ex-situ PLA-based composites, a PLA stock solution with a concentration of 100 mg/mL was prepared using THF solvent. A pure PANI solution (100 mg/mL) or a PANI solution (100 mg/mL) containing CFs (10, 30 and 50 mg/mL) was dispersed separately or added continuously in THF, followed by sonication in an ultrasonic bath for 1 h. Then, the PLA solution was mixed with equal volumes of the dispersed solutions of THF/PANI and THF/PANI/CFs to achieve a final PLA concentration of 50 mg/mL. The composite solutions were homogenized employing an ultrasonic processor/homogenizer (UP 400 S with 50% amplitude and 0.5 cycle) in an ice bath. The solution containing a ratio of the PLA solution/PANI solution (1:1) was labeled as PLA/PANI. Composite solutions containing PANI and CFs at different CFs loadings were termed PLA/PANI/$CFs_{0.1}$ for 10 mg/mL, PLA/PANI/$CFs_{0.3}$ for 30 mg/mL, and PLA/PANI/$CFs_{0.5}$ for 50 mg/mL of CFs, while the PLA stock solution without additives was nominated as neat PLA. All ratios were considered based on PLA.

Formulation of PLA-Based Films

Films made from PLA were created using the solvent casting technique. After assembling PLA-based composites with various ratios, the composite solutions were dropped onto a glass sheet with a diameter of 4 cm and stored at room temperature for 24 h. The created films were removed from the plate by dipping into deionized water once the THF solvent had evaporated [43, 44].

Characterization

The ultraviolet-visible absorption spectrum of the prepared PANI was measured using a UV-spectrophotometer (Type UV-2401PC) at room temperature in the region of 200–900 nm, with (DMSO) as a solvent and reference.

Thermo Scientific, Madison, WI, USA, equipped with an ATR attachment with a Ge crystal, was used to capture the FTIR spectra. The FTIR spectra were obtained with a resolution of 4 cm^{-1} in the region of 4000 to 650 cm^{-1}.

Scanning electron microscopy (SEM) using a JSM Jeol 6610 at an accelerated voltage of 15 kV was adopted to investigate the sample morphology. Just before the examination, a thin coating of gold was sputtered onto the samples to provide the required conductivity. AzTec software was applied to gather data and analyze the findings.

DSC measurements were performed using a Mettler-Toledo DSC 821e differential scanning calorimeter under nitrogen environment. In the region of 0–200 °C, the DSC measurements were conducted at a heating rate of 5 K min^{-1}. Before quenching and heating the samples to 200 °C at a rate of 5 K min^{-1}, the samples were initially heated to 200 °C to remove any prior thermal history. The glass transition temperature, measured at the onset of the step and at the midpoint of the specific heat increment, was calculated as the intercept between the baseline before the transition and the steepest tangent to the step. The melting and crystallization temperatures were chosen as the maximum values of the corresponding melting and crystallization endo- and exotherms.

Mechanical properties of the PLA-based films were investigated using a Dynamic Mechanical Analyzer DMAQ800 (TA Instruments, New Castle, DE, USA) at a

temperature range from −20 °C to 150 °C. A relatively low heating rate of 3 °C per minute was applied. Tensile mode with a frequency of 1 Hz with 20 μm strain deformation was applied. Two important quantities, such as storage modulus (E′) and damping factor (tan δ), were calculated for three individual measurements for each type of material.

The four-probe method, following the van der Pauw technique, was implemented to assess the electric resistivity and recalculated the electrical conductivity of the prepared films at room temperature using a high-precision electrometer (Keithley 6517B, USA).

The specific surface area (Brunauer–Emmett–Teller (BET) method) and the pore features of the synthesized films were evaluated by adsorption–desorption of N_2 at 77 K with a surface area analyzer model (BEL-Sorp-max, MicrotracBel Crop, Japan).

Results and Discussion

Spectral Characterization

Figure 1 shows the FTIR absorption bands of pure PLA, PLA/PANI and PLA/PANI/$CFs_{0.3}$ films. For PLA pellets, the absorption spectrum exhibits representative frequencies for C=O, $–CH_3$ asymmetric, $–CH_3$ symmetric, and C–O, at 1756, 2995, 2946 and 1080 cm^{-1}, respectively (Fig. 1a). Bending frequencies for asymmetric and symmetric ($–CH_3$) have been verified by the two frequencies at 1457 and 1363 cm^{-1}, respectively [45]. After adding PANI to PLA, a new peak frequency appears at 3200 cm^{-1}, which can be assigned to the hydrogen bonding from amine groups of PANI (Fig. 1b), similar to what is observed in the FTIR of pure PANI (Fig. S3). In addition, the quinonoid and the benzenoid moieties' stretching vibrations can be observed at 1557 cm^{-1}

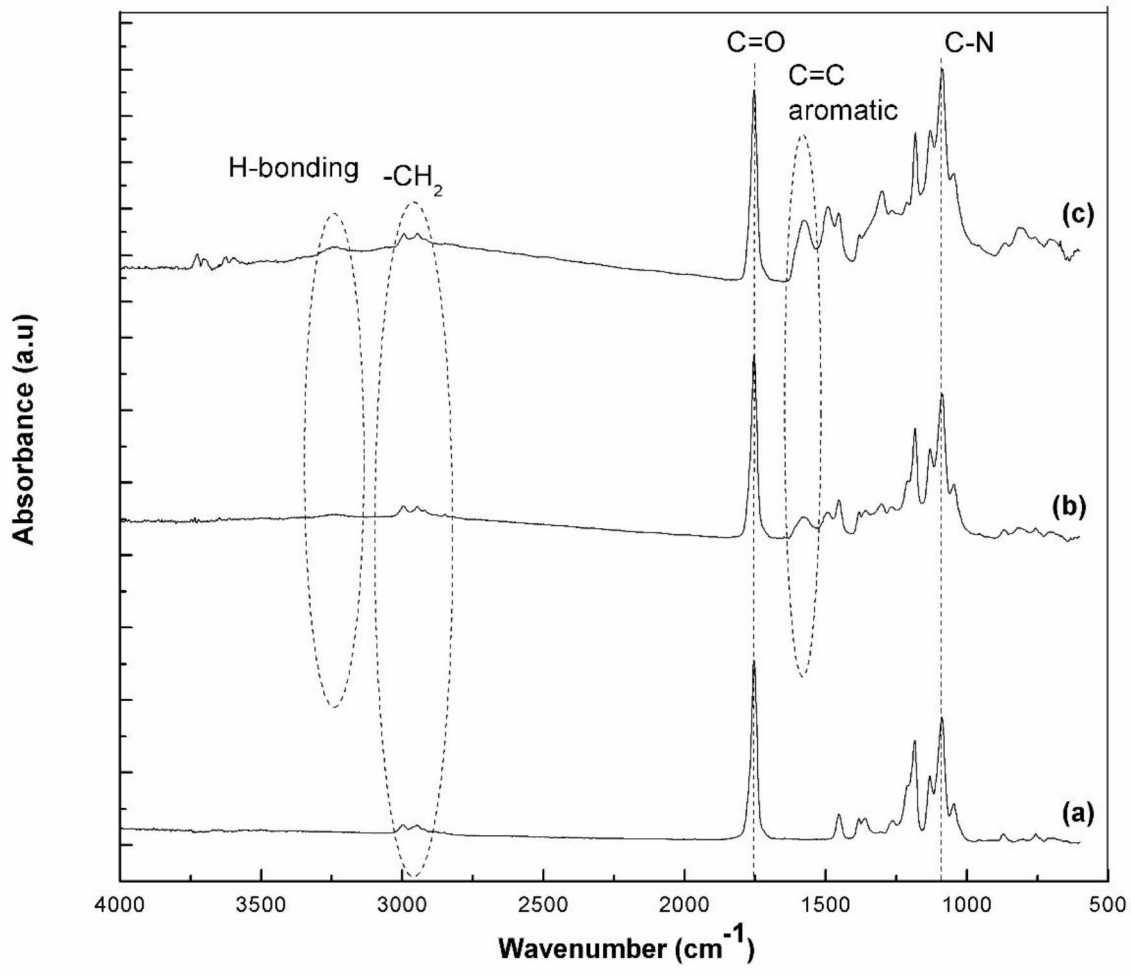

Fig. 1 FTIR spectra of (**a**) PLA pellets, (**b**) PLA/PANI film, and (**c**) PLA/PANI/$CFs_{0.3}$ film

and 1482 cm^{-1}, respectively [46]. The absorption band at about 1300 cm^{-1} in the spectrum corresponds to π-electron delocalization induced in the PANI polymer (polaronic structure), confirmed by a peak at 800 cm^{-1}. A small shoulder located at 1150 cm^{-1} from the vibration mode of the $–NH^{+}$ structure and C–N stretching bonds at 1058 cm^{-1} [47], visible in the spectra of pure PANI (Fig. S3), are overlapped by signals from PLA in the PLA/PANI blend. The addition of CFs to the PLA/PANI resulted in FTIR spectra almost identical to those of PLA/PANI (Fig. 1c).

Morphology of Fabricated Samples

SEM was performed to visualize the topographic details on the fiber surface to study the impact of carbonization temperature on the morphology, diameter, and carbon content of fabricated CFs. As depicted in Fig. 2a, the produced fibers have a spiral structure with an average diameter of 5–8 µm, consistent with the diameter cited by Shuguang Wang et al. [37], without any deformation of the assembled fibers after high-temperature carbonization. It also declared the typical hollow structures of the CFs produced from twisting of grown fibers [48].

The hollow structure enhanced the CFs' specific surface area [49]. This benefit was significant when CFs were operated as electrodes for super-capacitors because the inner surface could aid in charge storage [37]. Based on the SEM image, the wall thickness of CFs was estimated to be 850 nm. The EDX analysis of the produced CFs (Fig. 2b) shows that the material mainly consisted of carbon with an atomic fraction of 65%, followed by oxygen with an atomic fraction of 35%.

SEM was used for morphological analysis to estimate the PANI and CFs distribution throughout the PLA matrix. The micrographs are demonstrated in Fig. 3. Figure 3a evidences that the prepared PANI particles appear as grains varying from spherical to elongated shapes, interconnected heterogeneously with irregular diameters (2–7 µm). Figure 3b shows that the neat PLA film exhibited a smooth surface. After the insertion of PANI particles, the morphology changes to porous (Fig. 3c), showing a homogeneous covering of the PANI particles by PLA chains, probably due to H-bonding observed in FT- IR spectra at 3200 cm^{-1}. The porosity decreased after the addition of CFs. For lower loadings of CFs (PLA/PANI/$CFs_{0.1}$ and PLA/PANI/$CFs_{0.3}$), quite smooth surfaces were obtained, confirming homogeneous coverage of the CFs and PANI particles by PLA polymer (Fig. 3d and e). The smooth surface may also result from the effect of THF solvent, with which PANI and CFs can interact well. This leads to a good distribution of PANI and CFs in the PLA matrix. The good dispersion was attributed to effective interfacial adhesion between PLA and the inserted fillers. With higher CFs content (PLA/PANI/$CFs_{0.5}$), small amounts of agglomerated CFs can be observed (Fig. 3f). This result shows that the fibers cannot be distributed appropriately in the matrix when included at high portions because of their tendency to aggregate.

DSC Measurements

Differential scanning calorimetric (DSC) curves for PLA-based films were derived from both the first heating/cooling cycle and the second heating cycle to eliminate the thermal history of the samples [50]. The outcomes of thermal transition properties for PLA-based films, comprising the glass transition temperature (T_g), cold crystallization temperature (T_{cc}), melting temperature (T_m), and enthalpy (ΔH_m), are demonstrated in Table 1; Fig. 4, Figs. S5 and S6. The DSC thermograms exhibited two peaks in both the 1st and 2nd heating runs for neat PLA and PLA/PANI samples: the first for T_g and the second for T_m. As can be seen in Table 1, the addition of PANI shifts T_g to slightly higher temperatures, with almost no effect on T_m. The incorporation of PANI decreases the movement of PLA chain segments due to interfacial interactions through hydrogen bonding, thus acting as a barrier for relaxation processes [51]. On the other hand, PANI positively affects the crystallization of PLA, as indicated by ΔH_m values. In the 1st run, the consumed heat during melting is higher when recalculated to PLA content (34.2 Jg^{-1} for neat PLA and 43.2 Jg^{-1} for PLA in PLA/PANI). The difference in crystallization can be clearly seen from the 2nd heating run, where the ΔH_m value for neat PLA was significantly lower due to the fast cooling process, which did not allow sufficient crystallization. In contrast, in the presence of PANI during the 2nd heating run, the ΔH_m value reached almost 75% of the ΔH_m value from the 1st run, proving facilitation of crystallization even during fast cooling.

Incorporation of CFs into PLA/PANI blends led to decrease in T_g, indicating possible partial disruption of the PLA/PANI interactions. In addition, a third peak appeared during the 2nd heating runs, typical for cold crystallization (T_{cc}). The overall crystallinity slightly decreased compared to PLA/PANI, but ΔH_m values in the second runs were still higher than those determined for neat PLA. Observation of T_{cc} is typical for the composites where the filler acts as a nucleating agent, promoting the formation of crystals at the polymer/filler interface [52].

Dynamic Mechanical Thermal Analysis

The viscoelastic properties of neat PLA, PLA/PANI, and its composite films filled with CFs were evaluated using DMTA. The behavior of the damping factor (tan δ) and

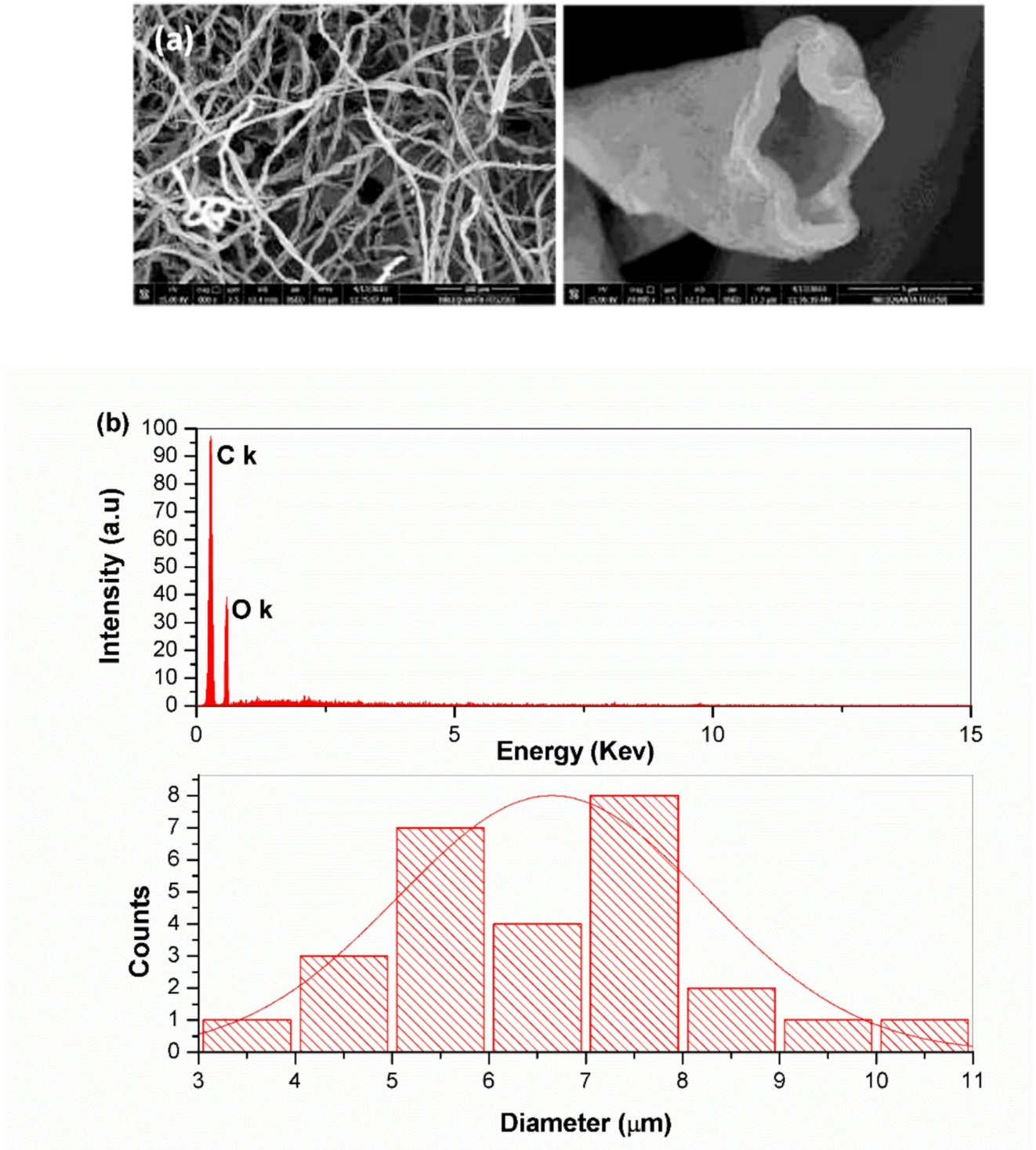

Fig. 2 (**a**) SEM, and (**b**) EDX with histogram diameter graphs for prepared CFs

storage modulus (E′) for all samples is compared in Fig. 5 (a and b), respectively. The concept of miscibility in thermodynamics is characterized by the existence of a single phase on the molecular level, represented by the single peak of the tan δ curve [53], which results from the transition of the polymer backbones from the glassy to rubbery state. This is generally determined as the peak value where the damping factor reaches its maximum, as revealed from Fig. 5a of the prepared films. The figure indicates that in all cases, there is a single T_g peak, implying that the system is homogenous.

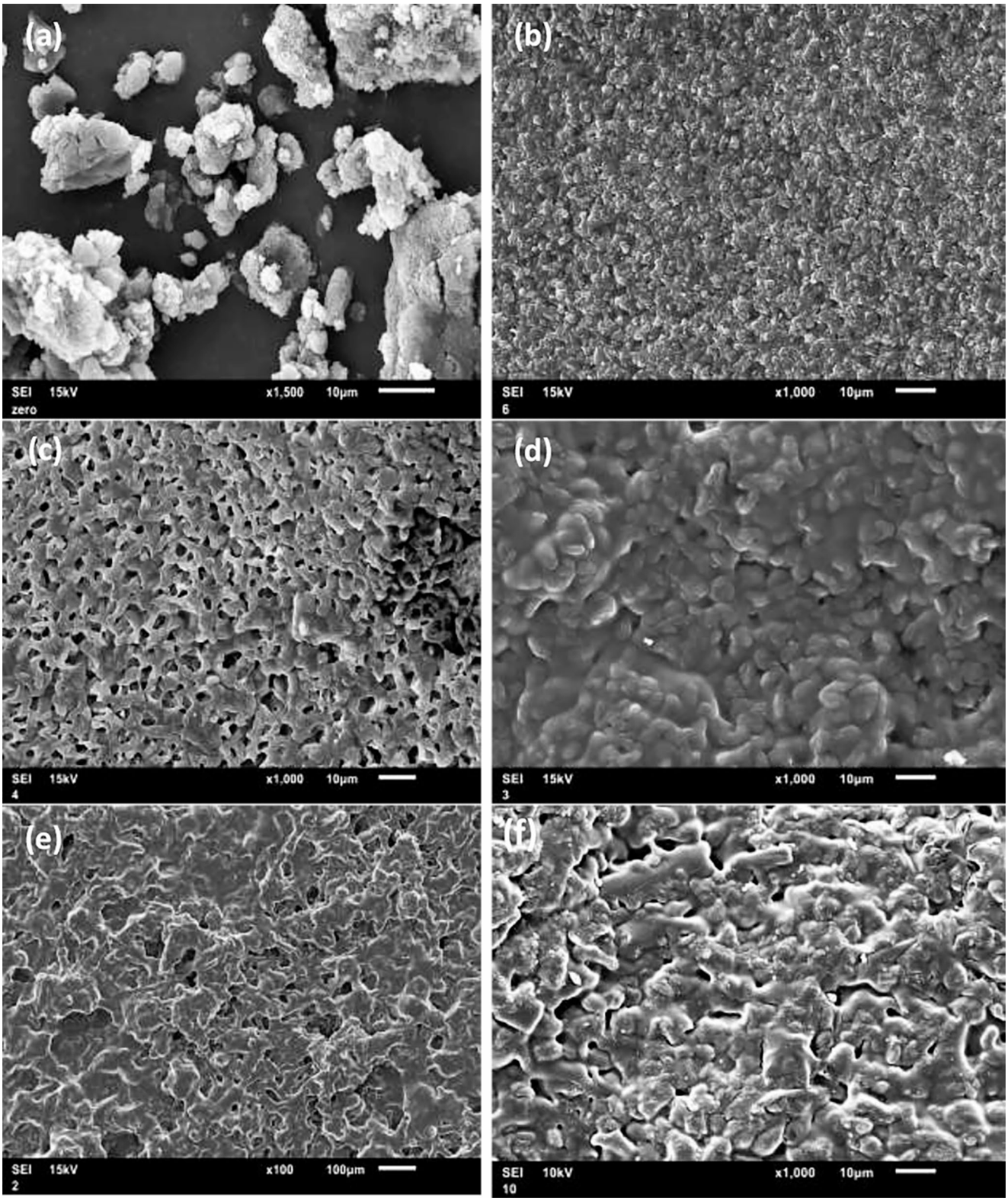

Fig. 3 SEM micrographs of (**a**) PANI particles, (**b**) Neat PLA film, (**c**) PLA/PANI film, (**d**) PLA/PANI/$CFs_{0.1}$, (**e**) PLA/PANI/$CFs_{0.3}$, and (**f**) PLA/PANI/$CFs_{0.5}$ films

Table 1 Thermal properties of PLA-based films determined from DSC and DMTA, such as cold crystallization temperature (T_{cc}), melting temperature (T_m), enthalpy (H_m), and glass transition (T_g) temperature

Sample	DSC				DMTA
	T_{cc} (°C)[a]	T_m (°C) 1st run / 2nd run	ΔH_m (Jg^{-1}) 1st run / 2nd run	T_g (°C)[a]	T_g (°C)
PLA	–	153.1 / 151.5	34.2 / 7.0	60.6	61.3
PLA/PANI	–	153.6 / 150.3	21.6 / 15.9	63.6	68.6
PLA/PANI/$CFs_{0.1}$	119.2	153.4 / 149.9	21.1 / 12.2	61.3	59.5
PLA/PANI/$CFs_{0.3}$	125.8	152.6 / 150.0	17.6 / 10.3	61.4	53.0
PLA/PANI/$CFs_{0.5}$	123.6	151.7 / 149.9	15.4 / 11.5	61.4	53.2

[a]determined from the second heating run

According to recorded DMTA data, the T_g values of neat PLA, PLA/PANI, and PLA/PANI/$CFs_{(0.1, 0.3, 0.5)}$ films were observed at 61.3 °C, 68.6 °C, 59.5 °C, 53 °C, and 53.2 °C, respectively. The trend of T_g values corresponds well with the DSC results. However, while the neat PLA film has a similar T_g value as measured by DSC, after mixing with PANI and in the presence of CFs, some differences in values were observed. The T_g of the PLA/PANI film shifted to a higher temperature, manifested by significant broadening of the glass transition region and a drop in the tan δ maximal intensity as a result of the incorporation of PANI particles into the polymer matrix, accompanied by decreased polymer segments mobility. The addition of CFs caused a decrease in the maximum T_g peak, shifting it to lower temperatures compared to neat PLA and PLA/PANI films. The addition of CFs seems to disrupt the PLA/PANI interactions without forming new interactions between the CFs and PLA, thus making PLA chains more mobile.

Figure 5b shows the dependence of E′ on temperature for all prepared samples. The changes in E′ are generally related to the interfacial adhesion within polymer multi-phase systems, as well as mutual interactions of particles, and provide information about material stiffness. The neat PLA film shows a plateau of E′ with the highest value at 25 °C before a sharp decline, indicating a transition from a glassy to a rubbery state [54, 55]. The addition of PANI into the PLA polymer structure led to a sharp decline in the E′ modulus in the glassy region (at 25 °C) before T_g, attributed to the reduction of strong inter-chain interactions between regularly arranged PLA chains. The incorporation of CFs into PLA/PANI led to slight increase in E′ compared to the

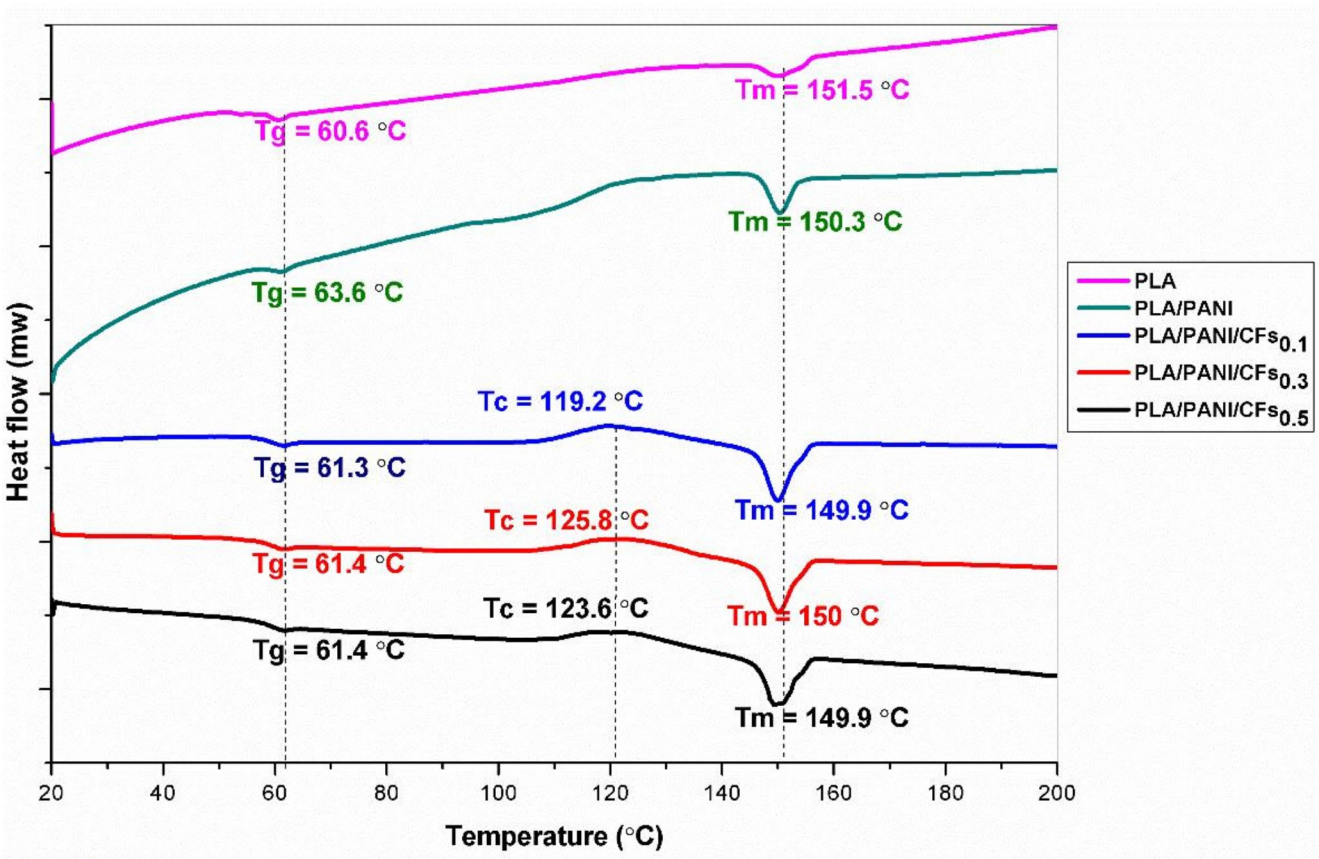

Fig. 4 2nd heating run from DSC thermograms of PLA-based films

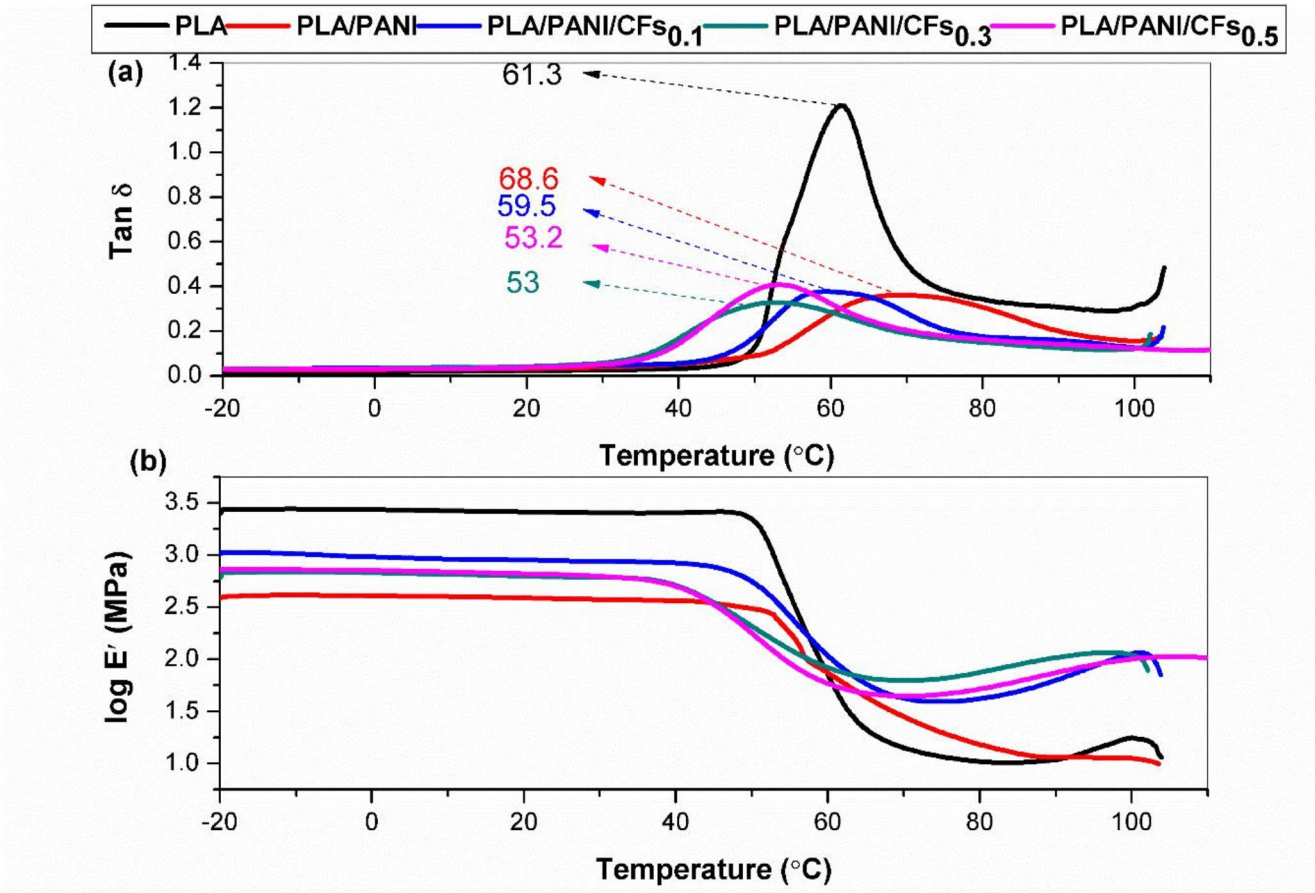

Fig. 5 Evolution of (**a**) damping factor (tan δ), and (**b**) log storage modulus (E′) with temperature for fabricated PLA-based films

unfilled blend due to the reinforcing effect of CFs, as is commonly observed for composites [56–58].

Electrical Conductivity Measurements

Major factors affecting polymer conductivity include chain length, chain ordering, and the degree of polymer conjugation [43]. It is likely that the addition of PANI and CFs to the composite will affect the electrical conductivity of fabricated PLA-based films. To analyze this effect, the electrical conductivity of PLA-based composite films with different CFs loadings was evaluated, as obvious in Fig. 6. As anticipated, the PLA film is a non-conductive polymer; however, the contribution of PANI in the PLA composite can provide the PLA/PANI film with conductive function (10^{-6} S/cm). This denotes that by positioning PANI between PLA chains, considerable electrical conductivity is achieved in the film [43]. The mobile carriers generated by the π-electronic system are responsible for PANI's electrical conductivity. An electric charge is created in the polymer chain by the removal of electrons from the valence band (positive charge) or the incorporation of electrons into the conduction band (negative charge), resulting in a significant change in the arrangement of atoms at the charge site and, ultimately, a change in electrical conductivity [59].

Figure 6 shows the increase in conductivity of PLA/PANI/CFs films regarding the CFs content. Carbon is the primary constituent of carbon fiber, and its molecular structure is similar to that of graphite. Because of this, it behaves like a metal with exceptionally high electrical conductivity [60]. The potential of graphite to conduct electricity is due to the existence of delocalized and free electrons on graphene sheets [61]. The conjugated system in CFs is stacked irregularly and amorphously, creating turbostratic layering. The gap between these sheets in a turbostratic layer arrangement is greater than that seen in graphite [62]. Filling the space between the fibers of CFs with PANI can boost electrical conductivity. It acts as an amplifier, facilitating electron movement by providing a channel for electrons to travel to neighboring conjugated sheets, thereby improving electrical conductivity.

Although the presence of CFs boosts electrical conductivity, an excess of CFs in the samples might slightly reduce it [44]. Conductivity data suggests a minimal ratio of CFs must be maintained in the PLA matrix to facilitate electron transport, with conductivity declining beyond this point.

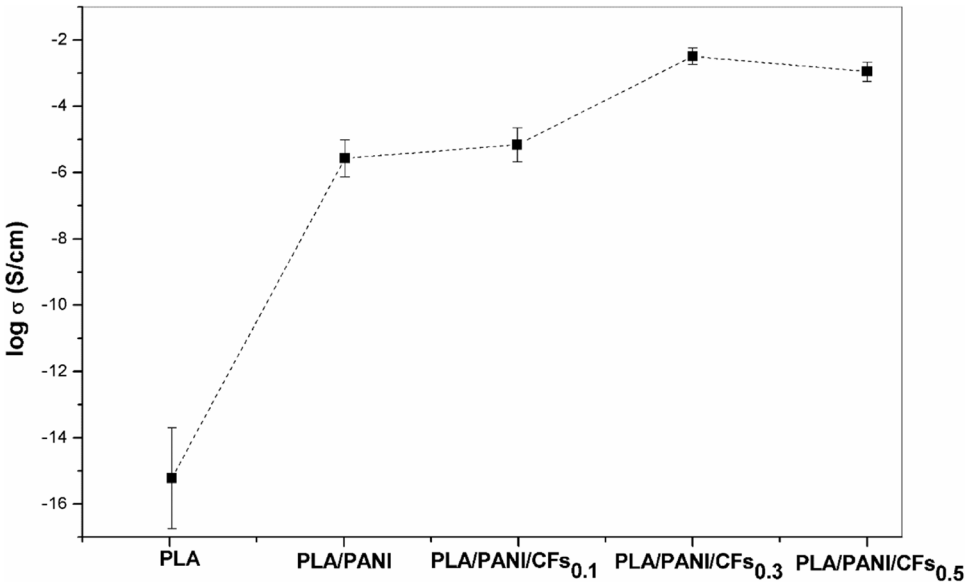

Fig. 6 Electrical conductivity of PLA-based films as a function of CFs content

$PLA/PANI/CFs_{0.3}$ presents the highest conductivity of 10^{-3} S/cm, which is slightly reduced in $PLA/PANI/CFs_{0.5}$. Thus, PLA/PANI/CFs films can serve as a cost-efficient electrically conductive material for device assembly techniques.

Effect of Various Factors on Adsorption

To surpass the mass transfer barrier of adsorbate particles among the aqueous and solid phases, it is essential to consider the initial dye concentration [63]. With a contact period of 60 min, a pH of 7, and a temperature of 20 °C, the percentage removal of dyes declined as the initial dye concentration rose from 50 to 100 mg/L, as obvious in Fig. 7a. This may be due to the filled active sites on the adsorbent surface and the increased mass transfer resistance attributed to higher adsorbate concentrations.

The pH of the solution is a key variables that severely impacts the adsorption conduct. It also affects the adsorbate standards, extent of ionization, and surface charge of the adsorbent material [64]. Since MG stability changes with pH, its pKa (6.9) [65] influences its behavior in the environment. Therefore, the sorption survey was conducted at pH levels between 2 and 7, where MG dye is stable and appears in colored form (green) [66], while maintaining an initial dye concentration of 50 $mg.L^{-1}$ at room temperature to explore the effects of pH. Figure 7b illustrates the correlation between the variation in pH of the solution and the amount of dye extracted by each studied PLA-based biosorbent film. The biosorption (%) of MG increased from 40.2, 22.8, and 49.2% to 98.2, 96, and 98% for PLA, PLA/PANI, and $PLA/PANI/CFs_{0.3}$, respectively, with increasing pH from 2 to 7. The limited biosorption of MG in very acidic solutions suggests a positive charge buildup on the biosorbent, preventing MG from adsorbing effectively [67]. The biosorbent surface becomes negatively charged as the pH of the solution rises, strengthening the electrostatic attraction between the positively charged MG cations and the PLA-based biosorbent film.

As illustrated in Fig. 7c, the adsorptive removal of dye onto produced adsorbents was assessed by adjusting the process duration from 5 to 60 min in 5-min intervals at an initial dye concentration of 50 mg/L, a solution pH of 7, and an adsorption temperature of 20 °C. When the contact period is extended up to 30 min, the adsorption increases quickly. This suggests that there was sufficient dye concentration in the solution to fill the adsorbent's empty active surfaces [68]. Nevertheless, after 30 min of contact time, the removal efficiency increased slowly up to 60 min, denoting a lack of accessible active sites on the adsorbent surface as the adsorbate tends to desorb into the liquid phase [69]. Therefore, it can be inferred that 60 min is sufficient contact time for the constructed adsorbent to achieve maximal removal from the dye solutions under the specified experimental conditions.

The adsorption process is significantly influenced by temperature. The majority of the adsorption process is exothermic, signifying that as temperature rises, the removal percentage tends to decrease. Figure 7d demonstrates that the percentage removal of MG dye declined as temperature increased (20, 30, 40, and 50 °C). The greatest removal was identified at 20 °C for an initial concentration of 50 mg/L and a contact duration of 60 min with a pH of 7. The findings indicated that the exothermic adsorption phenomenon and low adsorption temperatures were optimal for the MG dye to adsorb onto the produced adsorbents. At high temperatures, the active sites on adsorbent surface enlarge, and the dye molecules in the solution tend to return to the liquid phases [70]. Additionally, growing Brownian motion and

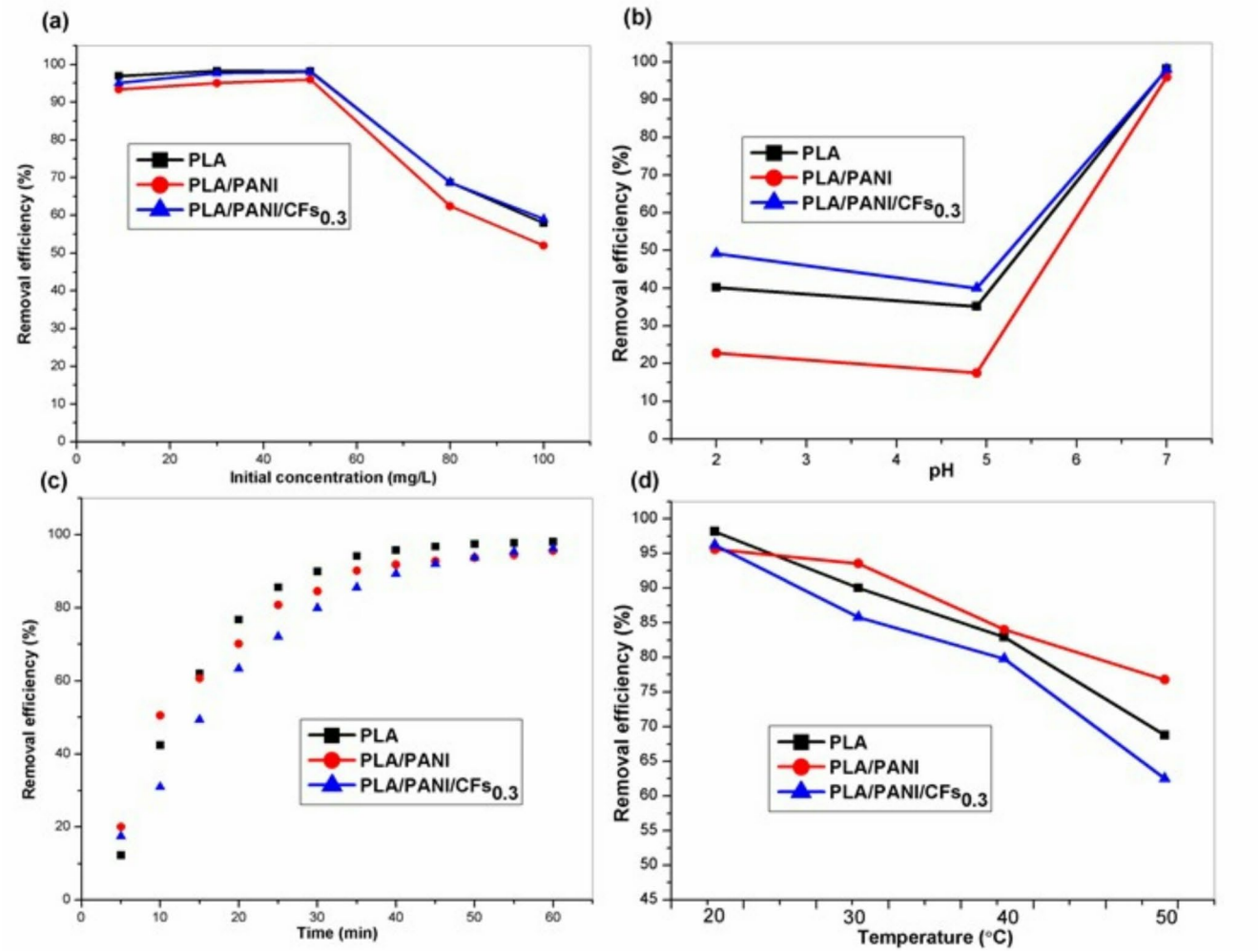

Fig. 7 Fluctuation of removal efficiency of MG with operating conditions, for all, the weight of tested films is 10 mg for (**a**) time 60 min, pH 7, T. 20 °C; (**b**) [MG] 50 mg/L, time 60 min, T. 20 °C; (**c**) [MG] 50 mg/L, pH 7, T. 20 °C; (**d**) [MG] 50 mg/L, pH 7, time 60 min

disruptions in the intermolecular hydrogen bonds between the dye and the adsorbents occur as the temperature rises [71].

Adsorption Equilibrium

An adsorption isotherm is commonly used to explain the equilibrium between the adsorbent and the adsorbate. To remove dye from eluents, it is imperative to determine the conceptual layout of the adsorption system by establishing the ideal correlation for the equilibrium curve. The equilibrium adsorption of MG dye (q_e against c_e) onto the prepared samples can be observed in Fig. 8.

To ascertain the adsorption approach and MG dye removal capability of the selected biosorbent films, Langmuir and Freundlich isotherm models were employed. Figure 9 (a and b) and Table 2 provide an overview of the correlation coefficients determined by fitting the experimental adsorption equilibrium data for MG removal by PLA-derived sample systems using the previously described adsorption isotherm models. According to the correlation coefficients (R^2), the findings showed that the Langmuir model fits the adsorption process of MG onto biosorbent films effectively. The Langmuir isotherm model assumes that chemisorption processes predominate with minimal physisorption and maximal adsorption relevant to a saturated monolayer of adsorbate onto the adsorbent surface. The maximum adsorption capacities towards MG were found to be 58.8, 54.3 and 60.1 mg/g adequately for PLA, PLA/PANI, and PLA/PANI/$CFs_{0.3}$. The highest ($Q_\circ$) was observed for PLA/PANI/$CFs_{0.3}$ owing to the broad and intense FT-IR negatively charged bands, which enhance its surface functionalization for dye removal via electrostatic bonds and high surface area measurements. Moreover, the values of R_L and (1/n) calculated from Langmuir and Freundlich parameters were lower than unity, signifying that the MG adsorption onto the samples

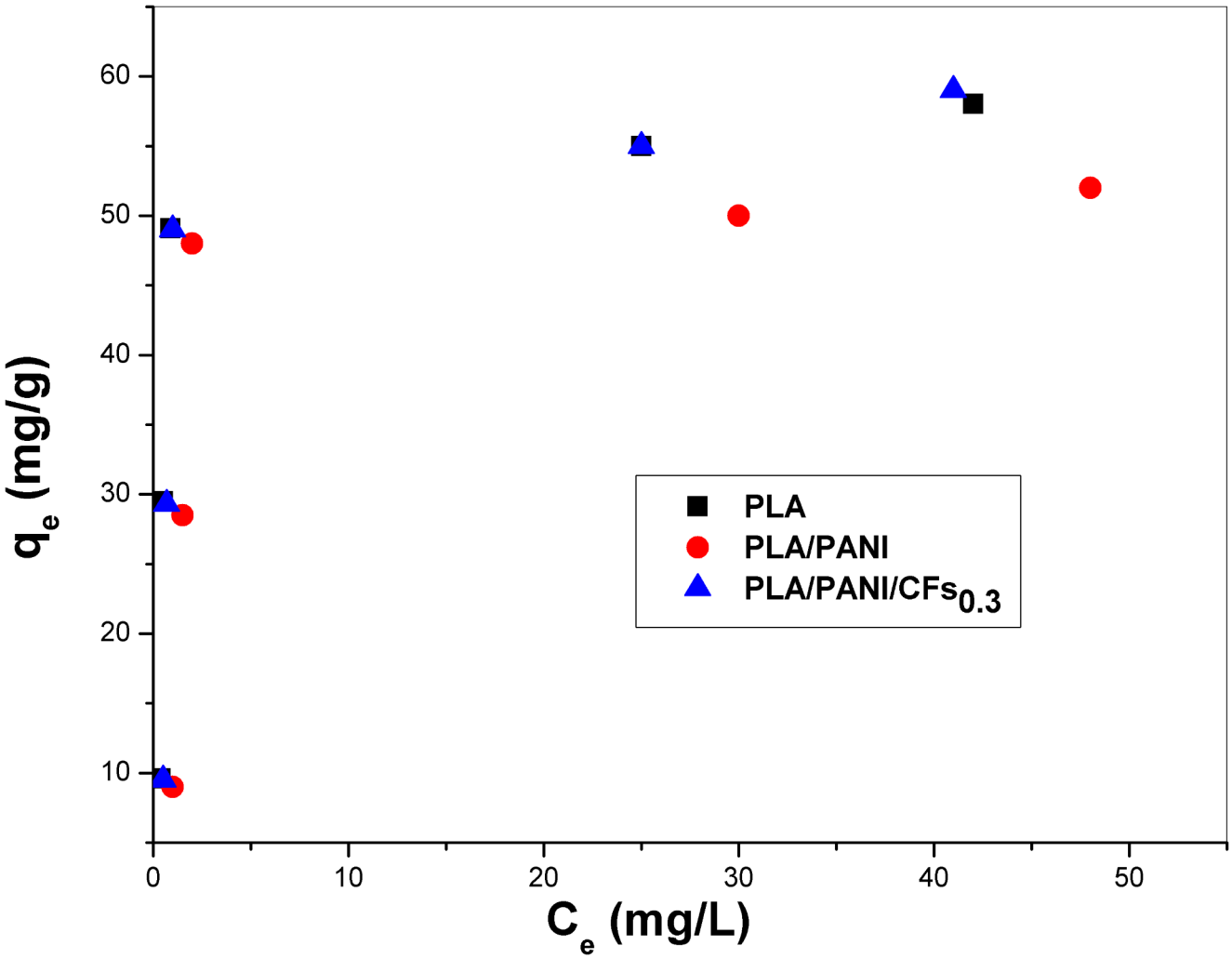

Fig. 8 Equilibrium isotherm plateau for MG dye biosorption

was effective. Table 3 manifests the adsorption capacity for MG removal of our equipped samples compared to other adsorbents.

Kinetic Modeling of Adsorption Process

The kinetics of MG adsorption on the produced films offer a spotlight on the entailed mechanism and rate-limiting stages, i.e., whether the adsorption is mass transfer controlled or reaction regulated. In this respect, there are various tools to investigate the mentioned adsorption, such as pseudo-first-order (PFO), pseudo-second-order (PSO), Elovich, intra-particle diffusion (IPD), and liquid film diffusion (LFD) kinetic frameworks. These are commonly utilized kinetic models for researching solid-liquid interactions and rely on adsorption capacity. Adsorption in the PFO kinetic model is governed by the mass transfer of the adsorbate to the location where actual adsorption takes place, while chemisorption is the rate-limiting stage in the PSO kinetic model [79]. The initial concentration of MG dye solution was 50 mg/L to reach optimum operating conditions for providing appropriate rate constants. The plots for MG dynamic considerations are showed in Fig. 10 (a, b). The adsorption capacity (q_e) and other important quantities such as k_1, k_2, α, β with statistical validation R^2 are presented in Table 4. If first-order kinetics are concerned, a linear dependence among $\ln(q_e\text{-}q_t)$ and t should be visible from Fig. 10. The values of k_1 and equilibrium adsorption capacity (q_e) were derived from the intercept and slope of the plots (Fig. 10a). The q_e values were consistent with the literature [80]. Furthermore, the PFO model exhibits a correlation coefficient (R^2) with very high values for the adsorption of MG molecules, close to unity [81]. Thus, the PFO model of PLA-derived films provides a better correlation for MG dye molecules. Notwithstanding, the correlation between dye concentration and the rate of adsorption exhibits non-linear behavior for the PSO model (Fig. S7). Since there is a relatively high difference between the R^2 coefficients for theoretical calculations and

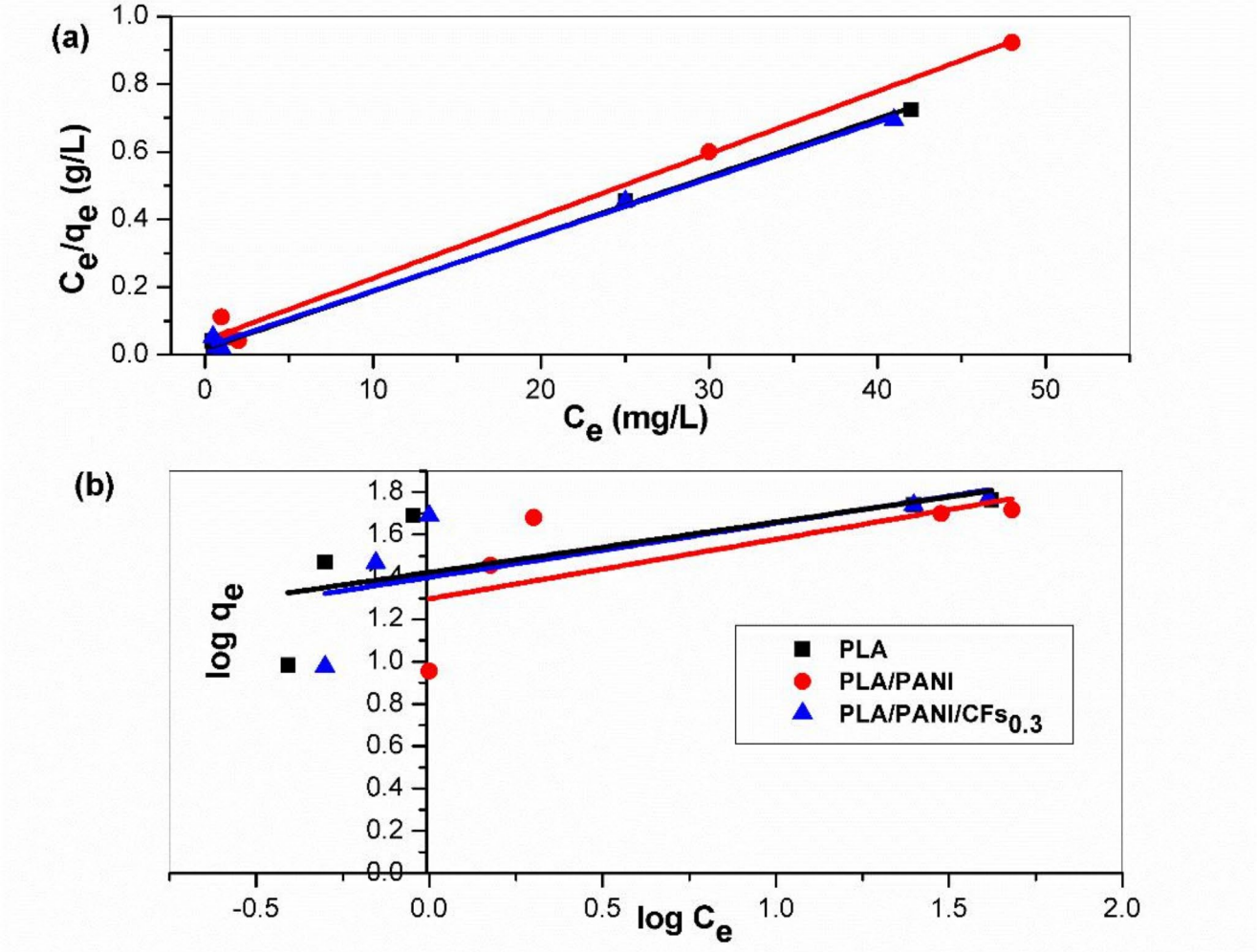

Fig. 9 Linear fitting of isotherm models of (**a**) Langmuir and (**b**) Freundlich for MG dye biosorption

Table 2 Langmuir and Freundlich isotherm constants for MG dye biosorption onto selected samples

Adsorbent	Langmuir isotherm model				Freundlich isotherm model		
	q_m (mg/g)	K_L (L/mg)	R_L	R^2	1/*n*	K_F	R^2
PLA	58.8	1	0.02	0.9976	0.28	19.8	0.2934
PLA/PANI	54.3	0.44	0.04	0.9909	0.26	25	0.3384
PLA/PANI/CFs$_{0.3}$	60.1	0.74	0.03	0.9955	0.24	26.4	0.33912

real experiments, it demonstrates that the MG dye molecules cannot be dedicated to PLA-derived films with the reaction mechanism of a second-order kinetic model.

As previously stated, the Elovich equation describes adsorption behavior that concurs with the nature of chemical adsorption [82]. As seen from Table 4, R^2 values are high (0.9365 to 0.9805), specifying that the adsorption process obeys the Elovich kinetic model. Despite these high values, they are comparatively lower than the findings from pseudo-first-order kinetics (0.9727 to 0.9955). Table 4 lists that the estimated values of α (initial adsorption rate) and the reciprocal of the desorption constant (1/β), which apparently indicates the number of sites available for adsorption. This suggests that the adsorption process is likely chemisorption, and the number of sites available for adsorption remains almost the same after modification with PANI and CFs [83].

The LFD model was implemented to investigate the potential for external diffusion. It highlights a relationship where values of -ln(1-F) are linearly related to values of t and the liquid film diffusion constant (K_{fd}). Additionally, q_t showed linear dependence with values of $t^{1/2}$, similar to the rate constant K_{id} for the intra-particle diffusion model (Table 5). The entire curves exhibited linearity and a zero

Table 3 Comparison of maximum adsorption capacities (q_m) reported in the literature for MG dye adsorption and our PLA-based films

Specimens	pH	T (°C)	q_m (mg/g)	References
Banana pseudo-stem fiber	7	25	26.5	[72]
Pleurotus ostreatus (a macro-fungus)	10	25	32.3	[73]
Wood apple shell	7.5	26	34.56	[74]
Rubber wood sawdust	–	32	36.45	[75]
Activated carbon of fig leaves	10	25	51.79	[76]
PLA/PANI	7	20	54.3	This study
PLA	7	20	58.8	This study
PLA/PANI/$CFs_{0.3}$	7	20	60.1	This study
Rattan sawdust	9–12	30	62.7	[77]
Treated ginger waste	9	30	84	[78]

Table 4 Kinetic parameters and correlation coefficients for MG removal by PLA-based films

Models	Parameters	PLA	PLA/PANI	PLA/PANI/$CFs_{0.3}$
Pseudo-first-order	q_e (exp) (mg/g)	49.1	48	49
	R^2	0.9878	0.9727	0.9955
	K_1 (min^{-1})	0.11	0.085	0.07
	q_e (model) (mg/g)	60.3	50.3	54.7
Pseudo-second-order	R^2	0.6846	0.9595	0.9378
	K_2 (g/mg.min)	$3.5\ x\ 10^{-4}$	$8.4\ x\ 10^{-4}$	$3.4\ x\ 10^{-4}$
	q_e (model) (mg/g)	84	65	81.4
Elovich	R^2	0.9365	0.9637	0.9805
	α (mg/g. min)	6	7	5.2
	β (g/mg)	0.06	0.07	0.057

intercept value at the origin, indicating that liquid film or IPD models designate the only rate-limiting phase [84].

Figures 11 (a and b) evidence that none of the plots passed through the origin without the y-intercept, with a high regression coefficient (R^2). The negative y-intercept for liquid diffusion model denotes the impact of high resistance of external film diffusion [85, 86]. This is related to the combined effect of film diffusion and intra-particle diffusion

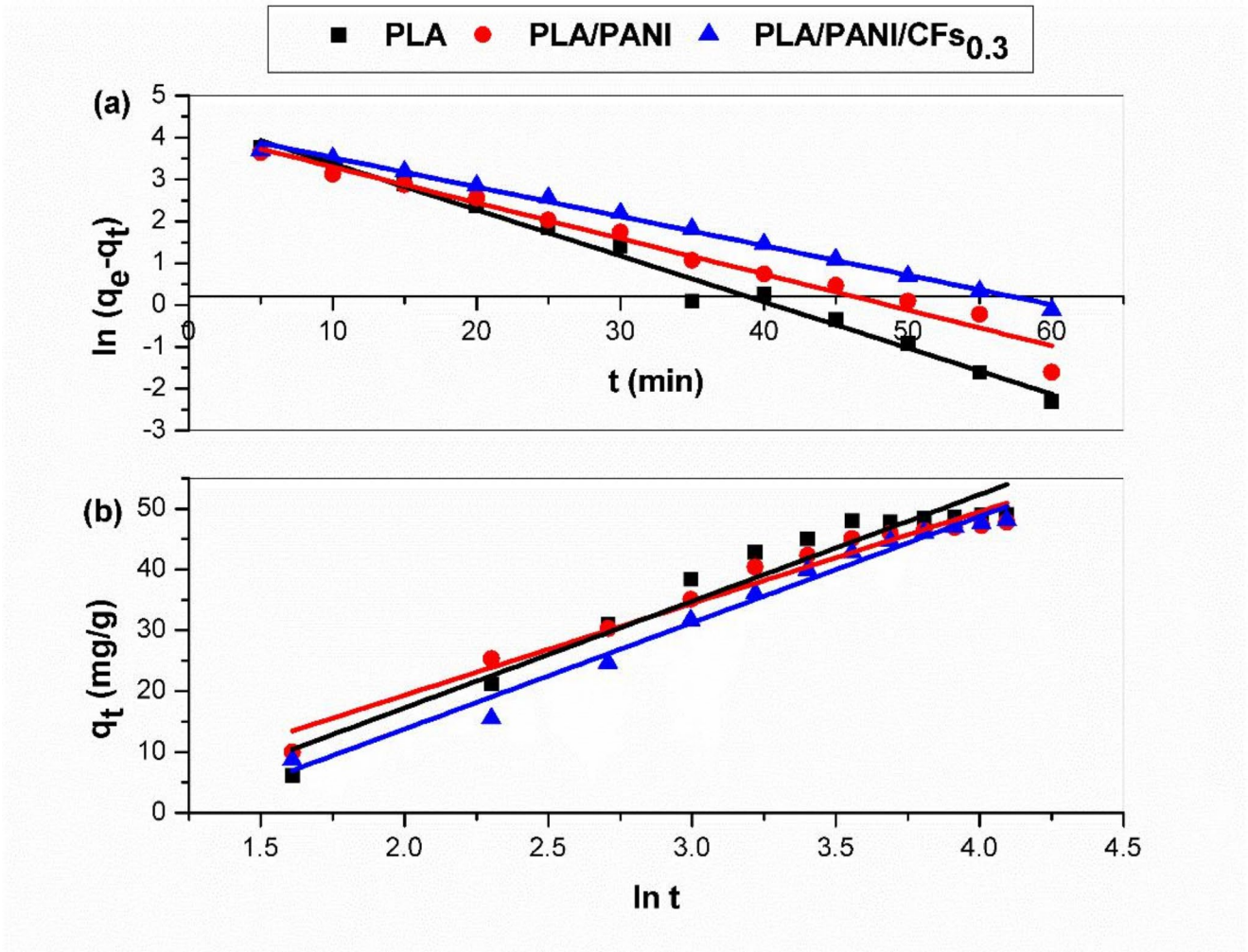

Fig. 10 Linear fitting of (**a**) pseudo-first-order, (**b**) Elovich kinetic models

Table 5 Mass transfer parameters and correlation coefficients for removal of MG onto PLA-based films

	Intra Particle Diffusion Model			Liquid Film Diffusion Model	
	K_{id} (mg/g.min$^{0.5}$)	C	R^2	K_{fd} (min^{-1})	R^2
PLA	7.2	0.61	0.822	0.076	0.9445
PLA/PANI	5	12.4	0.9298	0.094	0.979
PLA/PANI/$CFs_{0.3}$	7.4	−4.4	0.9384	0.093	0.969

with surface reaction control [86–88], which authenticates the difficulty in identifying the sole rate-determining step.

Thermodynamic Studies

A range of temperatures (293, 303, 313, and 323 K) was employed to examine the MG dye sorption onto PLA-based biosorbents. The values of ΔH° and ΔS° can be estimated from the slope and intercept of the plot of lnK vs. 1/T (Fig. 12), which are presented in Table 6. The fabricated biosorbents disclosed an exothermic reaction with the MG dye, as the process is stimulated by a decrease in temperature. This was verified by the negative results of ΔH° (−80.3, −52.3, and −74.3 kJ/mol) for PLA, PLA/PANI, and PLA/PANI/$CFs_{0.3}$, respectively. The solid/liquid interface decreasing randomness during the adsorption process is exhibited through the negative entropy value (-ΔS°) [89]. As well, at the designated temperatures, negative values of ΔG° illustrated that the MG dye adsorbed onto the adsorbents spontaneously [90].

BET-Analysis

The Brunauer-Emmett-Teller (BET) diagnostic criteria were employed to ascertain the specific surface area (S_{BET}) of the evaluated films. Furthermore, pore size distribution (PSD) curves corresponding to each sample were gathered using non-local density functional theory (NLDFT). The results are presented in Fig. S8. From S_{BET} measurements, it can be

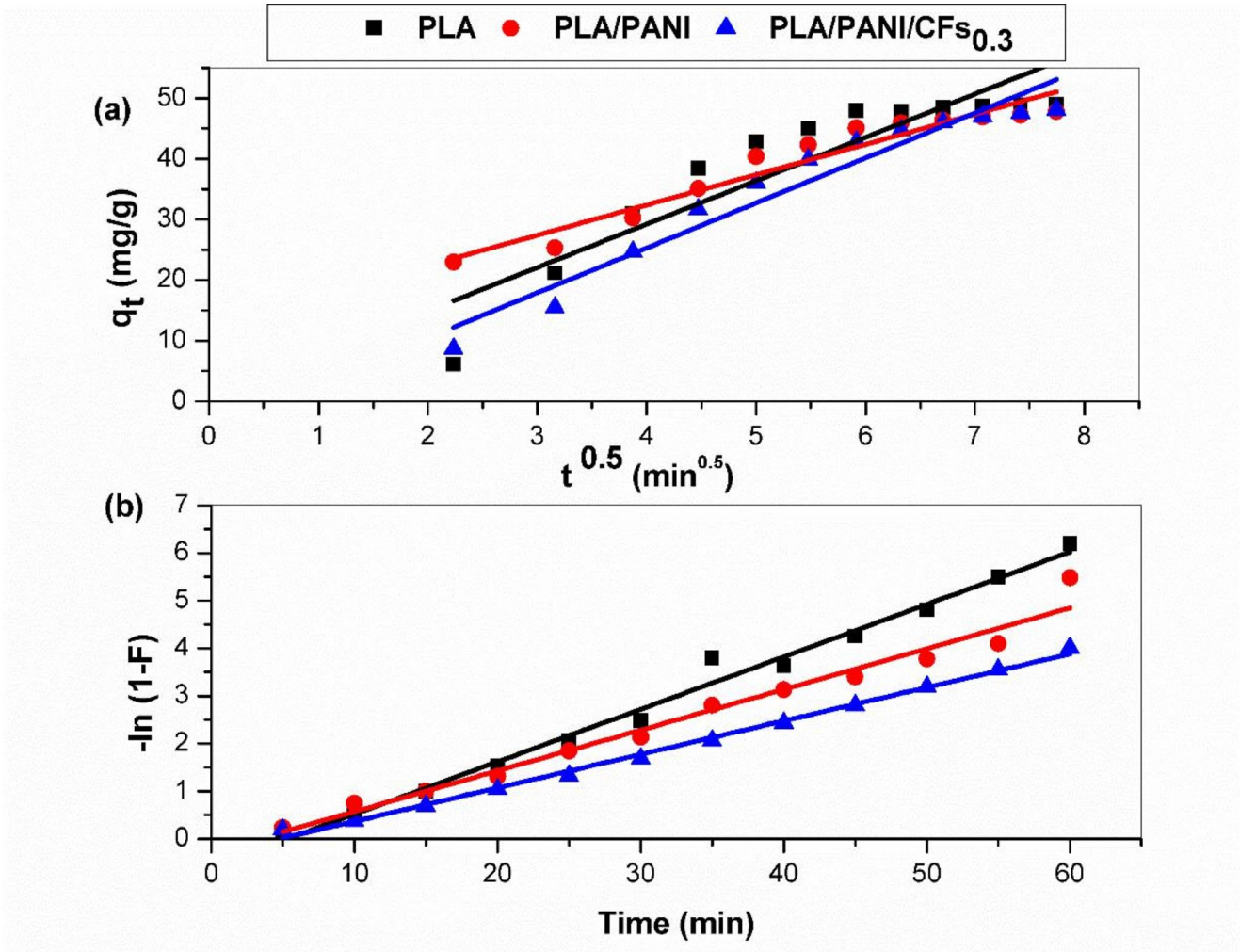

Fig. 11 (**a**) Intra-particle diffusion, and (**b**) liquid film-diffusion modeling of PLA-based films

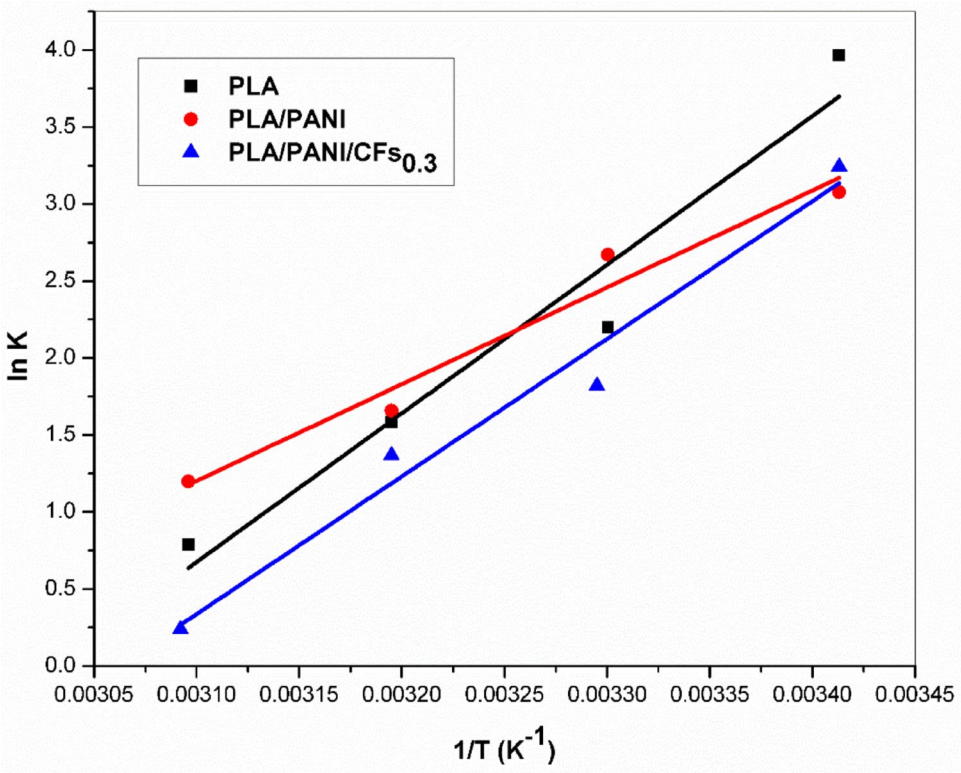

Fig. 12 Vant Hoff equation for adsorption performance of MG dye on fabricated films

Table 6 Thermodynamic specifications for the adsorption of MG dye on prepared films

Adsorbent	ΔH° (KJ/mole)	ΔS° (KJ/mole.K)	ΔG° (KJ/mole)			
			293K	303K	313K	323K
PLA	−80.3	−0.24	−9.1	−6.7	−4.2	−1.8
PLA/PANI	−52.3	−0.15	−7.7	−6.2	−4.7	−3.2
PLA/PANI/$CFs_{0.3}$	−74.3	−0.23	−4.5	−5.2	−2.9	−0.7

observed that the surface area is 2.1 $m^2.g^{-1}$ for PLA; however, there is an increase with the other prepared films, PLA/PANI (4.7 m^2/g) and PLA/PANI/$CFs_{0.3}$ (7.7 m^2/g). The disintegration and structural modification of PLA during the preparation of biocomposites are the main reasons for the increased surface area [91], with greater porosity resulting from the development of PANI and CFs, as depicted by SEM images [92]. The generated film's small surface area suggests blocked pores with little access to N_2 gas. The pore size distribution curves clarify the mesoporous nature of prepared films with pore diameters of 9.7, 19 and 8 nm for PLA, PLA/PANI and PLA/PANI/$CFs_{0.3}$, respectively.

Figures 13 (a and b) present the correlation between surface area (S_{BET}) with the removal (%) of MG dye and the electrical conductivity of the three selected films. The removal efficiency of MG dye in each sample shows an inconsistent relationship with the S_{BET} factor (Fig. 13a), where PLA with the lowest S_{BET} reveals the highest R% under optimum conditions for MG dye adsorption (T. 20 °C, [MG] 50 mg/L, time 60 min, and pH 7). However, with increasing S_{BET} for PLA/PANI, the R% decreased, and with incorporating CFs, it increased again. As a result, the removal of MG dye primarily depends on the functioning of the films and mechanisms generated by Van der Waals forces, which can attract the contaminants, π-π stacking, and electrostatic interactions rather than the overall porosity.

By contrast, Fig. 13b reveals that the S_{BET} greatly affects the electrical conductivity of the produced films. Films with a larger surface area may support a greater degree of expansion of the graphene sheets, increase the gap, allow more space for filling PANI, and lead to a greater chance of boosting electrical conductivity [93].

Regeneration Study

One of the most important aspects of economically viable water treatment was the reusability tests conducted on the PLA-based biosorbent films [94]. Washing the previously used adsorbents multiple times with double-distilled water revived them. The final adsorbent was dried at 80 °C and

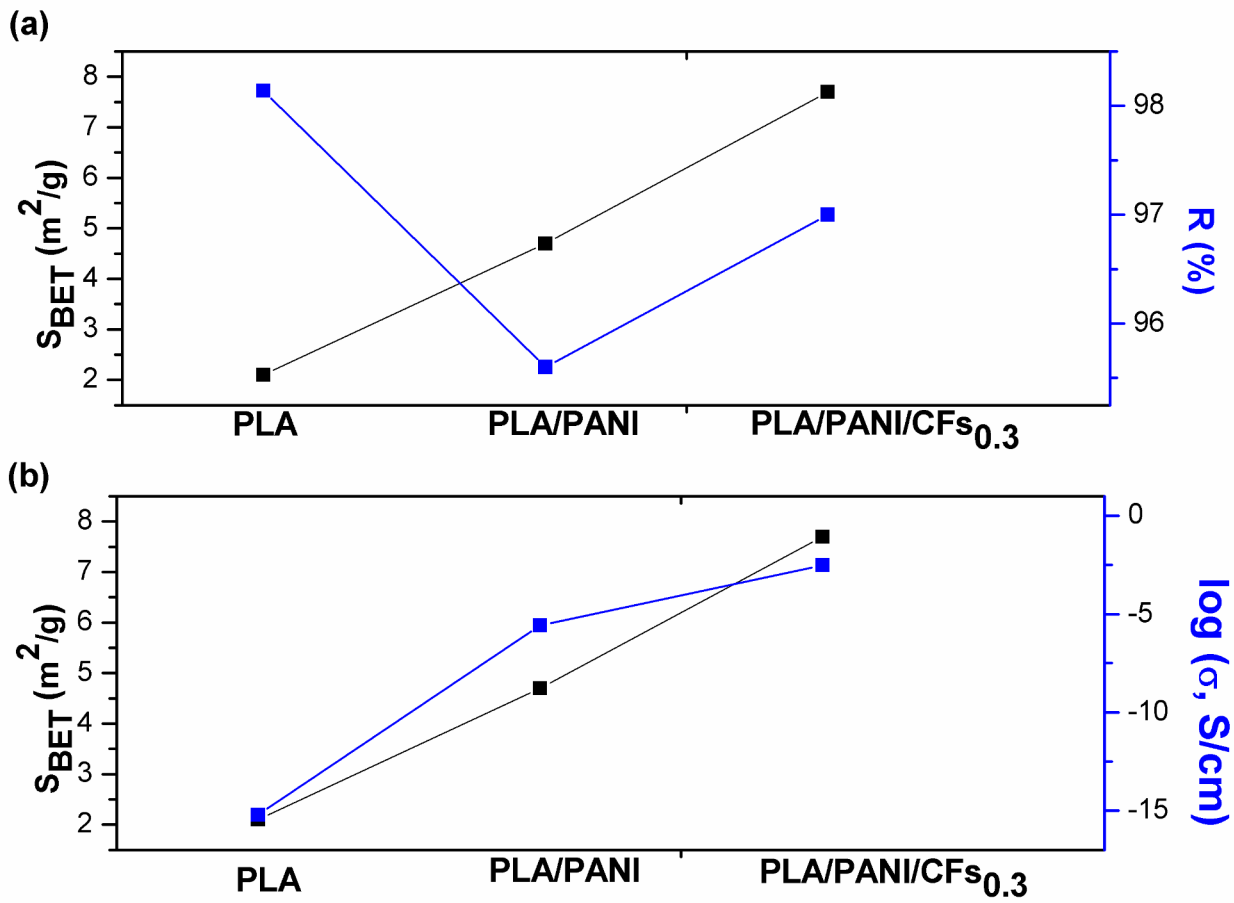

Fig. 13 Effect of the change of S_{BET} (m^2/g) on (**a**) the removal efficiency (%) of MG dye, and (**b**) the electrical conductivity of prepared films

reapplied up to six cycles at room temperature to decontaminate MG dye ([MG] 50 mg/L, pH 7, 60 min adsorption duration). The experimental data (Fig. 14) suggested that MG dye adsorption became somewhat less efficient as the number of cycles increased, indicating that H_2O regenerations had high recycling features. Throughout the first three regeneration cycles, MG biosorption capability was maintained at around 47 mg/g. After six consecutive cycles, the adsorption capacity of MG for PLA, PLA/PANI, and PLA/PANI/$CFs_{0.3}$ is 45, 43.8, and 44.8 mg/g, respectively. Consequently, PLA-based films can be exploited as an effective, affordable, and recyclable biosorbent to treat wastewater containing MG dye.

Effect of MG Concentration on Electric Conductivity

Finally, the potential applicability of the PLA/PANI/$CFs_{0.3}$ composite film as a sensor for MG concentration was investigated. The change in electrical conductivity of the film after adsorption of MG from solutions with various concentrations was determined. As clearly seen from Fig. 15, while the conductivity for the non-conductive PLA-film is negligibly affected by MG concentration, the conductivity of PLA/PANI/$CFs_{0.3}$ as a potential sensor decreased progressively with dye adsorption.

The decrease in conductivity is most likely caused by the disruption of the conducting pathways in the PLA/PANI/$CFs_{0.3}$ after MG adsorption. The observed changes in the sample's conductivity are promising proof of concept for further investigation of PLA-based conductive composites to potentially be used as dye detection sensors. It should be noted that under real environmental conditions, the concentration of the dye is usually significantly lower than the concentrations tested here. However, considering the high adsorption efficiency of MG below a concentration of 50 mg/L (see Fig. 7a), over time, a sufficiently high amount of MG will be adsorbed from the environment to affect the conductivity of the adsorbent film. Moreover, the decrease

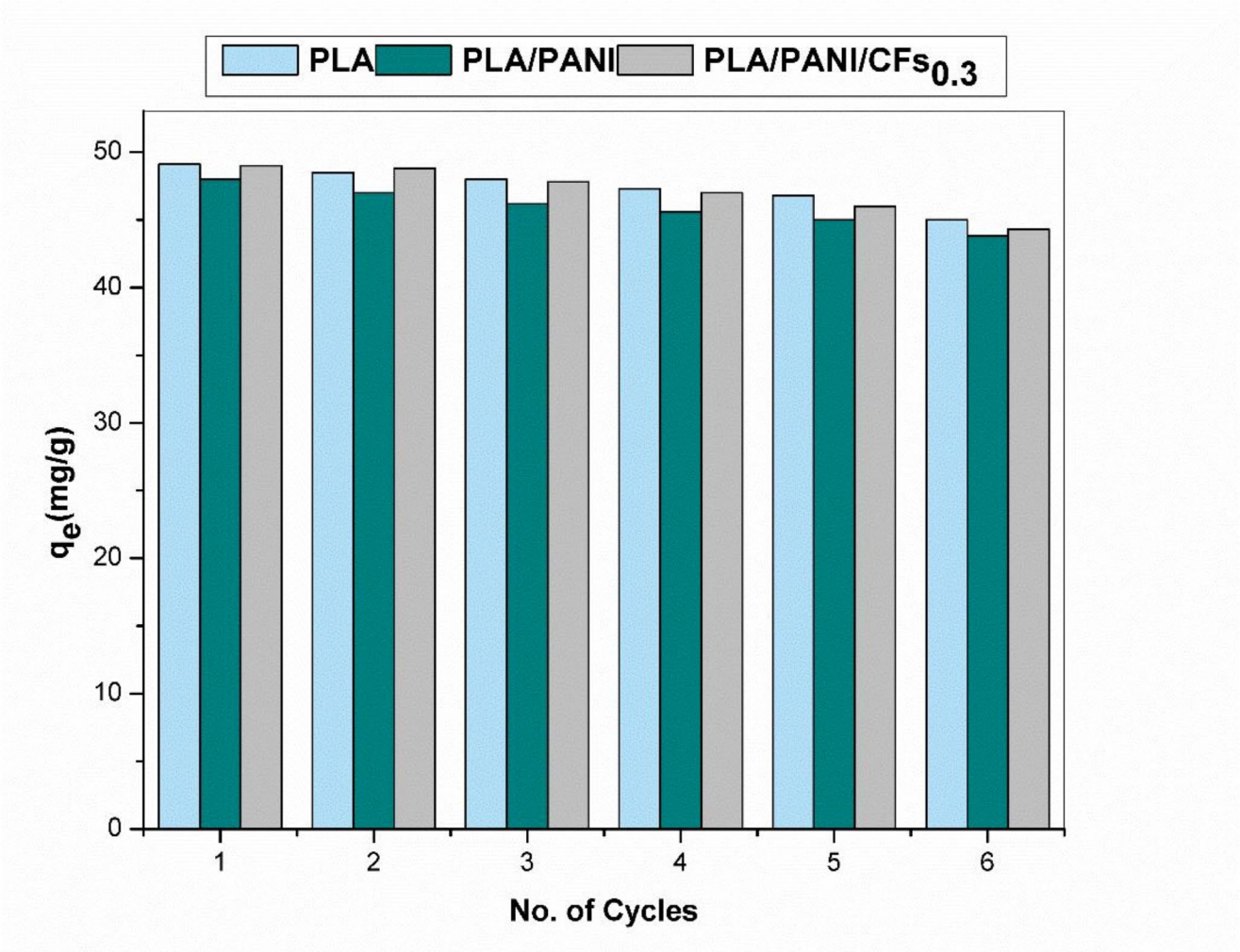

Fig. 14 Reusability cycles of MG dye biosorption by prepared films

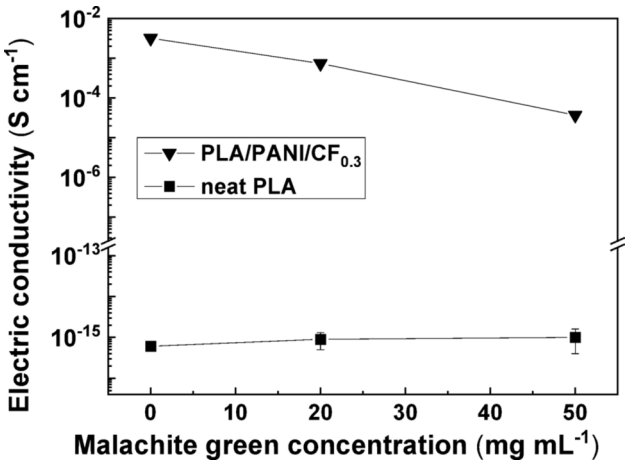

Fig. 15 Effect of MG concentration on electric conductivity of PLA and PLA/PANI/$CFs_{0.3}$ after 60 min of MG dye biosorption

in conductivity can signal the need to replace or regenerate the adsorbent to remain fully active in adsorption additional MG from water.

Conclusion

The present study describes the preparation of PLA-based films and their investigation as adsorbents for malachite green dye. In addition to pure PLA film, PLA/PANI blend, and PLA/PANI/CFs films with various CFs contents (1:1:0.1, 1:1:0.3, and 1:1:0.5) were prepared by ex-situ processing. A smooth film surface was stimulated by PLA/PANI/$CFs_{0.3}$, as evidenced by SEM micrographs. The hollow spiral CFs act as a nucleating agent, improving thermal stability, boosting the mobility of the amorphous phase, and increasing the storage modulus of PLA/PANI films. The prepared blend and composite films showed an increase in S_{BET} compared to pure PLA. The increased S_{BET} was accompanied by an

increase in electric conductivity, reaching the highest value of around 10^{-3} S/cm for PLA/PANI/$CFs_{0.3}$ with S_{BET} (7.7 m^2/g). The PLA/PANI/$CFs_{0.3}$ composite film also revealed a maximum adsorption capacity towards MG dye of 60.1 mg/g. Although a similar adsorption capacity was obtained also for pure PLA film, the advantage of PLA/PANI/$CFs_{0.3}$ was proved in its potential applicability as a sensor, showing a progressive decrease in electric conductivity with increased concentration of MG in water. This work also clearly showed that PLA-based films can be exploited as recyclable biosorbents to treat wastewater containing MG dye for at least six consecutive regeneration cycles.

Supporting Information

Optimization of synthesis and characterization of PANI; preparation of carbon fibers from waste cotton and their spectral characterization; DSC curves from 1st. run; adsorption studies – methods description and fitting results of adsorption equilibrium, kinetic and thermodynamic modeling; BET analysis. This material is available free of charge via the Internet.

Supplementary Information The online version contains supplementary material available at https://doi.org/10.1007/s10924-025-03563-y.

Acknowledgements The authors are thankful for financial support from projects VEGA 2/0042/25 and APVV-23-0534. Author M.M gratefully acknowledge to the Ministry of Education, Youth and Sports of the Czech Republic - DKRVO (RP/CPS/2024-28/003). Author K.M.A. also gratefully acknowledges the financial support of the Slovak Academic Information Agency (SAIA) within the National Scholarship Programme of The Slovak Republic.

Author Contributions K. M. A. did most of the experimental work and wrote the main manuscript text, M.M. did electric conductivity measurements and reviewed the manuscript, K.M. did dynamic mechanical thermal analysis and reviewed the manuscript, J.M supervised the research work and reviewed the manuscript.

Funding Open access funding provided by The Ministry of Education, Science, Research and Sport of the Slovak Republic in cooperation with Centre for Scientific and Technical Information of the Slovak Republic

Data Availability The authors declare that the data supporting the findings of this study are available within the paper and its Supplementary Information files. Should any raw data files be needed in another format they are available from the corresponding author upon reasonable request.

Declarations

Competing Interests The authors declare no competing interests. Authors disclose no financial or non-financial interests that are directly or indirectly related to the work submitted for publication. All listed authors have approved the manuscript before submission, including the names and order of authors.

References

1. Pete S, Kattil RA, Thomas L (2021) Polyaniline-multiwalled carbon nanotubes (PANI- MWCNTs) composite revisited: an efficient and reusable material for Methyl orange dye removal. Diam Relat Mater 117:108455. https://doi.org/10.1016/j.diamond.2021.108455
2. Sutar SS, Patil PJ, Tamboli AS, Patil DN, Apine OA, Jadhav JP (2019) Biodegradation and detoxification of malachite green by a newly isolated bioluminescent bacterium Photobacterium leiognathi strain MS under RSM optimized culture conditions. Biocatal Agric Biotechnol 20:101183. https://doi.org/10.1016/j.bcab.2019.101183
3. Fideles RA, Ferreira GMD, Teodoro FS, Adarme OFH, da Silva LHM, Gil LF, Gurgel LVA (2018) Trimellitated sugarcane Bagasse: A versatile adsorbent for removal of cationic dyes from aqueous solution. Part I: batch adsorption in a monocomponent system. J Colloid Interface Sci 515:172–188. https://doi.org/10.1016/j.jcis.2018.01.025
4. Dehghani MH, Yetilmezsoy K, Salari M, Heidarinejad Z, Yousefi M, Sillanpää M (2020) Adsorptive removal of cobalt(II) from aqueous solutions using multi-walled carbon nanotubes and γ-alumina as novel adsorbents: modelling and optimization based on response surface methodology and artificial neural network. J Mol Liq 299:112154. https://doi.org/10.1016/j.molliq.2019.112154
5. Raval NP, Shah PU, Shah NK (2016) Adsorptive amputation of hazardous Azo dye congo red from wastewater: a critical review. Environ Sci Pollut Res 23:14810–14853. https://doi.org/10.1007/s11356-016-6970-0
6. Mahmoodi NM, Sadeghi U, Maleki A, Hayati B, Najafi F (2014) Synthesis of cationic polymeric adsorbent and dye removal isotherm, kinetic and thermodynamic. J Ind Eng Chem 20:2745–2753. https://doi.org/10.1016/j.jiec.2013.11.002
7. Horodytska O, Cabanes A, Fullana A (2019) The handbook of environmental chemistry. Springer, Heidelberg
8. Riaz S, Fatima N, Rasheed A, Riaz M, Anwar F, Khatoon Y (2018) Metabolic engineered biocatalyst: A solution for PLA based problems. Hindawi 2018(1–9). https://doi.org/10.1155/2018/1963024
9. Naser AZ, Deiab I, Darras BM (2021) Poly(lactic acid) (PLA) and polyhydroxyalkanoates (PHAs), green alternatives to petroleum-based plastics: a review. RSC Adv 11:17151–17196. https://doi.org/10.1039/d1ra02390j
10. Naeem S, Baheti V, Militky J, Ali A (2019) Multifunctional polylactic acid composites filled with activated carbon particles obtained from acrylic fibrous wastes. Polym Compos 40:578–590. https://doi.org/10.1002/pc.24695

11. Shen XJ, Yang S, Shen JX, Ma JL, Wu YQ, Zeng XL, Fu SY (2019) Improved mechanical and antibacterial properties of silver-graphene oxide hybrid/polylactid acid composites by in-situ polymerization. Ind Crops Prod 130:571–579. https://doi.org/10.1016/j.indcrop.2019.01.018
12. Pan F, Chen L, Jiang Y, Xiong L, Min L, Xie J, Qi J, Xiao H, Chen Y, De Hoop CF (2018) Bio-based UV protective films prepared with polylactic acid (PLA) and Phoebe Zhennan extractives. Int J Biol Macromol 119:582–587. https://doi.org/10.1016/j.ijbiomac.2018.07.189
13. Krupa I, Mahmoud A, Sobolciak P, Popelka A, Mrlik M, Minarik A, Gasmi S, Ouederni M, Adham S (2022) A novel alternative to free oil remediation and recovery: foamy absorbents designed from low molecular paraffinic waste. Sep Purif Technol 302:122118. https://doi.org/10.1016/j.seppur.2022.122118
14. Mallakpour S, Behranvand V (2021) Polyurethane sponge modified by alginate and activated carbon with abilities of oil absorption, and selective cationic and anionic dyes clean-up. J Clean Prod 312:127513. https://doi.org/10.1016/j.jclepro.2021.127513
15. Shah HUR, Ahmad K, Parveen HANS, Ashfaq M, Rauf A, Aziz T (2021) Water stable graphene oxide metal-organic frameworks composite (ZIF-67@GO) for efficient removal of malachite green from water. Food Chem Toxicol 154:112312. https://doi.org/10.1016/j.fct.2021.112312
16. Zhang K-N, Lei Z-L, Lü Q-F (2024) Flower-like ZnO modified TiO_2@$Ti_3C_2T_x$ composite for efficient adsorption of malachite green and oil-water separation. J Clean Prod 447:141632. https://doi.org/10.1016/j.jclepro.2024.141632
17. Aijaz MO, Yang SB, Karim MR, Alnaser IA, Alahmari AD, Almubaddel FS, Assaifan AK (2023) Preparation and characterization of electrospun Poly(lactic acid)/Poly(ethylene glycol)–b–poly(propylene glycol)–b–poly(ethylene glycol)/Silicon Dioxide Nanofibrous Adsorbents for Selective Copper (II) Ions Removal from Wastewater. Membr (Basel) 13:1–16. https://doi.org/10.3390/membranes13010054
18. Samadi A, Xie M, Li J, Shon H, Zheng C, Hao SZ, Hao (2021) Polyaniline - based adsorbents for aqueous pollutants removal: A review. Chem Eng J 418:129425. https://doi.org/10.1016/j.cej.2021.129425
19. Stejskal J (2022) Recent advances in the removal of organic dyes from aqueous media with conducting polymers, polyaniline and polypyrrole, and their composites. Polym (Basel) 14:1–22. https://doi.org/10.3390/polym14194243
20. Park SS, Lee YS, Lee SW, Repo E, Kim TH, Park Y, Hwang Y (2023) Facile surface treatment of 3D-Printed PLA filter for enhanced graphene oxide doping and effective removal of cationic dyes, polymers (Basel). 15 1–20. https://doi.org/10.3390/polym15020269
21. Sattar M, Hayeeye F, Chinpa W, Sirichote O (2017) Preparation and characterization of Poly (lactic acid)/activated carbon composite bead via phase inversion method and its use as adsorbent for Rhodamine B in aqueous solution. J Environ Chem Eng 5:3780–3791. https://doi.org/10.1016/j.jece.2017.07.007
22. Zhang S, Shao T, Kose HS, Tanju K (2010) Adsorption of aromatic compounds by carbonaceous adsorbents: A comparative study on granular activated carbon, activated carbon fiber, and carbon nanotubes. Environ Sci Technol 44:6377–6383. https://doi.org/10.1021/es100874y
23. Mosnáčková K, Danko M, Šišková A, Falco LM, Janigová I, Chmela Š, Vanovčanová Z, Omaníková L, Chodák I, Mosnáček J (2017) Complex study of the physical properties of a poly(lactic acid)/poly(3-hydroxybutyrate) blend and its carbon black composite during various outdoor and laboratory ageing conditions. RSC Adv 7. https://doi.org/10.1039/c7ra08869h
24. Stejskal J, Trchová M, Bober P, Humpolíček P, Kašpárková V, Sapurina I, Shishov MA, Varga M (2015) Conducting Polymers: Polyaniline. Encycl Polym Sci Technol. 1–44. https://doi.org/10.1002/0471440264.pst640
25. Gospodinova N, Terlemezyan L (1998) Conducting polymers prepared by oxidative polymerization: polyaniline. Prog Polym Sci 23:1443–1484. https://doi.org/10.1016/S0079-6700(98)00008-2
26. Winter B, Meys R, Bardow A (2021) Towards aromatics from biomass: prospective life cycle assessment of bio-based aniline. J Clean Prod 290:1–36. https://doi.org/10.1016/j.jclepro.2021.125818
27. Gernot J, Magnus J, Moussa AS (2019) Production of aniline via anthranilate. U S Patent No 10,173,969. 8 Jan., 2019.
28. Samadi A, Wang Z, Wang S, Nataraj SK, Kong L, Zhao S (2023) Polyaniline-based adsorbents for water treatment: roles of low-cost materials and 2D materials. Chem Eng J 478:147506. https://doi.org/10.1016/j.cej.2023.147506
29. Ansari R, Mosayebzadeh Z (2011) Application of polyaniline as an efficient and novel adsorbent for Azo dyes removal from textile wastewaters. Chem Pap 65:1–8. https://doi.org/10.2478/s11696-010-0083-x
30. Chowdhury A-N, Jesmeen SR, Hossain MM (2004) Removal of dyes from water by conducting polymeric adsorbent. Polym Adv Technol 4:121–129. https://doi.org/10.1002/pat.521Citations
31. Majhi D, Patra BN (2020) Polyaniline and sodium alginate nanocomposite: A pH-responsive adsorbent for the removal of organic dyes from water. RSC Adv 10:43904–43914. https://doi.org/10.1039/d0ra08125f
32. Shahabuddin S, Sarih NM, Ismail FH, Shahid MM, Huang NM (2015) Synthesis of Chitosan grafted-polyaniline/Co_3O_4 nanocube nanocomposites and their photocatalytic activity toward methylene blue dye degradation. RSC Adv 5:83857–83867. https://doi.org/10.1039/c5ra11237k
33. Gong M, Zhao Q, Dai L, Li Y, Jiang T (2017) Fabrication of polylactic acid/hydroxyapatite/graphene oxide composite and their thermal stability, hydrophobic and mechanical properties. J Asian Ceram Soc 5:160–168. https://doi.org/10.1016/j.jascer.2017.04.001
34. Llorens E, Calderón S, Del Valle LJ, Puiggalí J (2015) Polybiguanide (PHMB) loaded in PLA scaffolds displaying high hydrophobic, biocompatibility and antibacterial properties. Mater Sci Eng C 50:74–84. https://doi.org/10.1016/j.msec.2015.01.100
35. Mazur RL, Oliveira PC, Rezende MC, Botelho EC (2014) Environmental effects on viscoelastic behavior of carbon Fiber/PEKK thermoplastic composites. J Reinf Plast Compos 3:749–757
36. Mohammadizadeh M, Fidan I (2019) Thermal analysis of 3d printed continuous fiber reinforced thermoplastic polymers for automotive applications, in: Proc 30th Annu Int Solid Free Fabr Symp - An Addit Manuf Conf,: pp. 899–906
37. Wang S, Ren Z, Li J, Ren Y, Zhao L, Yu J (2014) Cotton-based Hollow carbon fibers with high specific surface area prepared by ammonia etching for supercapacitor application. RSC Adv 4:31300–31307. https://doi.org/10.1039/c4ra04383a
38. Khatooni H, Peighambardoust SJ, Foroutan R, Mohammadi R, Ramavandi B (2023) Adsorption of methylene blue using sodium carboxymethyl cellulose-g-poly (acrylamide-co-methacrylic acid)/Cloisite 30B nanocomposite hydrogel. J Polym Environ 31:297–311. https://doi.org/10.1007/s10924-022-02623-x
39. Peighambardoust SJ, Aghamohammadi-Bavil O, Foroutan R, Arsalani N (2020) Removal of malachite green using carboxymethyl cellulose-g-polyacrylamide/montmorillonite nanocomposite hydrogel. Int J Biol Macromol 159:1122–1131. https://doi.org/10.1016/j.ijbiomac.2020.05.093
40. Safarzadeh H, Peighambardoust SJ, Peighambardoust SH (2023) Application of a novel sodium alginate-graft-poly(methacrylic acid-co-acrylamide)/montmorillonite nanocomposite hydrogel

for removal of malachite green from wastewater. J Polym Res 30. https://doi.org/10.1007/s10965-023-03531-x
41. Pakdel PM, Peighambardoust SJ, Foroutan R, Arsalani N, Aghdasi HN (2022) Decontamination of Fuchsin dye by carboxymethyl cellulose - graft - poly (acrylic acid - co - itaconic acid)/carbon black nanocomposite hydrogel. Int J Biol Macromol 222:2083–2097. https://doi.org/10.1016/j.ijbiomac.2022.10.007
42. Pakdel PM, Peighambardoust SJ, Arsalani N, Aghdasinia H (2022) Safranin-O cationic dye removal from wastewater using carboxymethyl cellulose-grafted-poly(acrylic acid-co-itaconic acid) nanocomposite hydrogel. Environ Res 212. https://doi.org/10.1016/j.envres.2022.113201
43. Wang X, Tang Y, Zhu X, Zhou Y, Hong X (2020) Preparation and characterization of polylactic acid/polyaniline/nanocrystalline cellulose nanocomposite films. Int J Biol Macromol 146:1069–1075. https://doi.org/10.1016/j.ijbiomac.2019.09.233
44. Ceregatti T, Pecharki P, Pachekoski WM, Becker D, Dalmolin C (2017) Electrical and thermal properties of PLA/CNT composite films. Rev Mater 22. https://doi.org/10.1590/S1517-707620170003.0197
45. Chieng BW, Ibrahim NA, Yunus WMZW, Hussein MZ (2014) Poly(lactic acid)/poly(ethylene glycol) polymer nanocomposites: effects of graphene nanoplatelets. Polym (Basel) 6:93–104. https://doi.org/10.3390/polym6010093
46. Sambasevam KP, Mohamad S, Phang SW (2015) Effect of Dopant concentration on polyaniline for hydrazine detection. Mater Sci Semicond Process 33:24–31. https://doi.org/10.1016/j.mssp.2015.01.008
47. Chiam YS, Mohamad Ahad IZ, Wadi Harun S, Gan SN, Phang SW (2016) Effects of the Dopant ratio on polyaniline coated fiber Bragg grating for pH detection. Synth Met 211:132–141. https://doi.org/10.1016/j.synthmet.2015.11.026
48. Jagdale P, Koumoulos EP, Cannavaro I, Khan A, Castellino M, Dragatogiannis DA, Tagliaferro A, Charitidis CA (2017) Towards green carbon fibre manufacturing from waste cotton: A microstructural and physical property investigation. Manuf Rev 4:1–9. https://doi.org/10.1051/mfreview/2017008
49. Cao S, Wu Z, Sun Q, Zhang W, Beysen S, Wang S, Shaymurat T, Zhang M, Duan H (2021) Gas sensing properties of cotton-based carbon fibers and ZnO/carbon fibers regulated by changing carbonization temperatures. Sens Actuators B Chem 337:129818. https://doi.org/10.1016/j.snb.2021.129818
50. Pracella M, Haque MMU, Puglia D (2014) Morphology and properties tuning of PLA/cellulose nanocrystals bio-nanocomposites by means of reactive functionalization and blending with PVAc. Polym (Guildf) 55:3720–3728. https://doi.org/10.1016/j.polymer.2014.06.071
51. Han W, Ren J, Xuan H, Ge L (2018) Controllable degradation rates, antibacterial, free-standing and highly transparent films based on polylactic acid and Chitosan. Elsevier B V. https://doi.org/10.1016/j.colsurfa.2018.01.022
52. Al-Samhan M, Al-Attar F, Al-Fadhli J, Al-Shamali M (2021) The influence of nano caco3 on nucleation and interface of Pp nano composite: matrix processability and impact resistance. Polym (Basel) 13:1389. https://doi.org/10.3390/polym13091389
53. Lafferty SV, Newton JM, Podczeck F (2002) Dynamic mechanical thermal analysis studies of polymer films prepared from aqueous dispersion. Int J Pharm 235:107–111. https://doi.org/10.1016/S0378-5173(01)00973-5
54. Kim S, Kim H, Kim H, Lee HH (2006) Effect of Bio-Scavengers on the curing behavior and bonding properties of Melamine-Formaldehyde resins. Macromol Mater Eng 291:1027–1034. https://doi.org/10.1002/mame.200600213
55. Park B, Kim J (2008) Dynamic mechanical analysis of Urea–Formaldehyde resin adhesives with different Formaldehyde-to-Urea molar ratios. J Appl Polym Sci 108:2045–2051. https://doi.org/10.1002/app.27595
56. Vignesh S, Shanmugam V, Kumar VJ (2022) Comparing the storage modulus of treated and untreated Calotropis gigantea reinforced polymer composites. In: 14th Int Conf Math Actuar Sci Comput Sci Stat (MACS), IEEE. https://doi.org/10.1109/MACS56771.2022.10023012
57. Cordin M, Bechtold T, Pham T (2018) Effect of fibre orientation on the mechanical properties of polypropylene–lyocell composites. Cellulose 25:7197–7210. https://doi.org/10.1007/s10570-018-2079-6
58. Khan ZI, Mohamad Z, Rahmat AR, Habib U (2021) Synthesis and characterization of composite materials with enhanced thermo-mechanical properties for unmanned aerial vehicles (Uavs) and aerospace technologies. Pertanika J Sci Technol 29:2003–2015. https://doi.org/10.47836/pjst.29.3.15
59. Abdolsattari P, Rezazadeh-Bari M, Pirsa S (2022) Smart film based on polylactic acid, modified with Polyaniline/ZnO/CuO: investigation of physicochemical properties and its use of intelligent packaging of orange juice. Food Bioprocess Technol 15:2803–2825. https://doi.org/10.1007/s11947-022-02911-3
60. Alarifi IM (2019) Investigation the conductivity of carbon fiber composites focusing on measurement techniques under dynamic and static loads. J Mater Res Technol 8:4863–4893. https://doi.org/10.1016/j.jmrt.2019.08.019
61. Martín-Martínez FJ, Fias S, Van Lier G, De Proft F, Geerlings P (2012) Electronic structure and aromaticity of graphene nanoribbons. Chem - Eur J 18:6183–6194. https://doi.org/10.1002/chem.201103977
62. Joshi K, Arefev MI, Zhigilei LV (2019) Generation and characterization of carbon fiber microstructures by atomistic simulations. Carbon N Y 152:396–408. https://doi.org/10.1016/j.carbon.2019.06.014
63. Rahim MR, Haris MM (2019) Chromium (VI) removal from neutral aqueous media using banana trunk fibers (BTF)-reinforced chitosan - based film, in comparison with BTF, Chitosan, Chitin and activated carbon. SN Appl Sci 1:1180. https://doi.org/10.1007/s42452-019-1206-9
64. Imamoglu M, Tekir O (2008) Removal of copper (II) and lead (II) ions from aqueous solutions by adsorption on activated carbon from a new precursor hazelnut husks. Desalination 228:108–113
65. Singh H, Chauhan G, Jain AK, Sharma SK (2016) Adsorptive potential of agricultural wastes for removal of dyes from aqueous solutions. J Environ Chem Eng 5:122–135
66. Ngah WSW, Fatinathan S (2008) Adsorption of Cu(II) ions in aqueous solution using chito- San beads, Chitosan -GLA beads and Chitosan– alginate beads. Chem Eng J 143:62–72
67. Vasanth Kumar K, Ramamurthi V, Sivanesan S (2006) Biosorption of malachite green, a cationic dye onto pithophora Sp., a fresh water algae. Dye Pigment 69:102–107. https://doi.org/10.1016/j.dyepig.2005.02.005
68. Jawad AH, Abdulhameed AS (2020) Mesoporous Iraqi red Kaolin clay as an efficient adsorbent for methylene blue dye: adsorption kinetic, isotherm and mechanism study. Surf Interfac 18:100422. https://doi.org/10.1016/j.surfin.2019.100422
69. Yap PS, Priyaa V (2019) Removal of crystal Violet and acid green 25 from water using Kaolin. IOP Conf Ser Mater Sci Eng. https://doi.org/10.1088/1757-899X/495/1/012052
70. Aragaw TA, Alene AN (2022) A comparative study of acidic, basic, and reactive dyes adsorption from aqueous solution onto Kaolin adsorbent: effect of operating parameters, isotherms, kinetics, and thermodynamics. Emerg Contam 8:59–74. https://doi.org/10.1016/j.emcon.2022.01.002
71. Prajapati AK, Mondal MK (2019) Hazardous As(III) removal using nanoporous activated carbon of waste Garlic stem as

adsorbent: kinetic and mass transfer mechanisms. Korean J Chem Eng 36:1900–1914. https://doi.org/10.1007/s11814-019-0376-x
72. Neha G, Kushwaha A, Chattopadhyaya M (2011) Kinetics and thermodynamics of malachite green adsorption on banana pseudo-stem fibers. J Chem Pharm Res 3:284–296
73. Chen Z, Deng H, Chen C, Yang Y, Xu H (2014) Biosorption of malachite green from aqueous solutions by pleurotus ostreatus using Taguchi method. J Environ Heal Sci Eng 12:1–10. https://doi.org/10.1186/2052-336X-12-63
74. Sartape AS, Mandhare AM, Jadhav VV, Raut PD, Anuse MA, Kolekar SS (2017) Removal of malachite green dye from aqueous solution with adsorption technique using limonia acidissima (wood apple) shell as low cost adsorbent. Arab J Chem 10:S3229–S3238. https://doi.org/10.1016/j.arabjc.2013.12.019
75. Kumar KV, Sivanesan S (2007) Isotherms for malachite green onto rubber wood (Hevea brasiliensis) sawdust: comparison of linear and non-linear methods. Dye Pigment 72:124–129
76. Gebreslassie YT (2020) Equilibrium, kinetics, and thermodynamic studies of malachite green adsorption onto Fig (Ficus cartia) leaves. J Anal Methods Chem 2020:1–11. https://doi.org/10.1155/2020/7384675
77. Hameed B, El-Khaiary M (2008) Malachite green adsorption by Rattan sawdust: isotherm, kinetic and mechanism modeling. J Hazard Mater 159:574–579
78. Kuma R (2010) Adsorption studies of hazardous malachite green onto treated ginger waste. J Environ Manage 91:1032–1038
79. Crini G, Badot P-M (2008) Application of Chitosan, a natural aminopolysaccharide, for dye removal from aqueous solutions by adsorption processes using batch studies: A review of recent literature. Prog Polym Sci 33:399–447. https://doi.org/10.1016/j.progpolymsci.2005.07.001
80. Abas KM, Fathy NA (2023) Sodalite zeolitic materials produced from coal fly Ash for removal of congo red dye from aqueous solutions. Int J Environ Sci Technol November 1–20. https://doi.org/10.1007/s13762-023-05347-0
81. Hashem A, Al-Kheraije K (2013) Chemically modified cornulaca monacantha biomass for bioadsorption of hg (II) from contaminated water: adsorption mechanism. J Env Prot 4:280–286
82. Wu FC, Tseng RL, Juang RS (2009) Characteristics of Elovich equation used for the analysis of adsorption kinetics in dye-chitosan systems. Chem Eng J 150:366–373. https://doi.org/10.1016/j.cej.2009.01.014
83. Aworanti OA, Agarry SE (2017) Kinetics, isothermal and thermodynamic modelling studies of hexavalent chromium ions adsorption from simulated wastewater onto Parkia biglobosa-Sawdust derived Acid-Steam activated carbon. Appl J Environ Eng Sci 3:58–76
84. Bulut E, Özacar M, Şengil IA (2008) Equilibrium and kinetic data and process design for adsorption of congo red onto bentonite. J Hazard Mater 154:613–622. https://doi.org/10.1016/j.jhazmat.2007.10.071
85. McKay G (1983) The adsorption of dyestuffs from aqueous solutions using activated carbon, III: intraparticle diffusion processes. J Chem Technol Biotechnol 33:196e204. https://doi.org/10.1002/jctb.504330406
86. Alakhras F, Bel Hadj Hmida ES, Anastopoulos I, Trabelsi Z, Mabrouk W, Ouerfelli N, Fauvarque JF (2021) Diffusion analysis and modeling of kinetic behavior for treatment of Brine water using electrodialysis process. Water Sci Eng 14:36–45. https://doi.org/10.1016/j.wse.2020.05.002
87. Rudzinski W, Plazinski W (2008) Kinetics of solute adsorption at solid/solution in- terfaces: on the special features of the initial adsorption kinetics. Langmuir 24:6738–6744
88. Tan KL, Hameed BH (2017) Insight into the adsorption kinetics models for the removal of contaminants from aqueous solutions. J Taiwan Inst Chem Eng 74:21–47. https://doi.org/10.1016/j.jtice.2017.01.024
89. Al-Ahmary KM (2013) Kinetics and thermodynamic study of malachite green adsorption on seeds of dates. Int J Basic Appl Sci 2:27–37. https://doi.org/10.14419/ijbas.v2i1.477
90. Al-Harby N.F., Albahly E.F., Mohamed N.A. (2021) Kinetics, isotherm and thermodynamic studies for efficient adsorption of congo red dye from aqueous solution onto novel Cyanoguanidine-Modified Chitosan adsorbent. Polym (Basel) 13:1–32. https://doi.org/10.3390/polym13244446
91. Nair V, Panigrahy A, Vinu R (2014) Development of novel chitosan-lignin composites for adsorption of dyes and metal ions from wastewater. Chem Eng J 254:491–502. https://doi.org/10.1016/j.cej.2014.05.045
92. Babaei-Ghazvini A, Acharya B (2023) The effects of aspect ratio of cellulose nanocrystals on the properties of all CNC films: tunicate and wood CNCs. Carbohydr Polym Technol Appl 5:100311. https://doi.org/10.1016/j.carpta.2023.100311
93. Ravindran AR, Feng C, Huang S, Wang Y, Zhao Z, Yang J (2018) Effects of graphene nanoplatelet size and surface area on the AC electrical conductivity and dielectric constant of epoxy nanocomposites. Polym (Basel) 10:19–35. https://doi.org/10.3390/polym10050477
94. Ahmed MB, Zhou JL, Ngo HH, Guo W, Chen M (2016) Progress in the Preparation and application of modified Biochar for improved contaminant removal from water and wastewater. Bioresour Technol 214:836–851. https://doi.org/10.1016/j.biortech.2016.05.057